SANDIA REPORT
SAND2010-7333
Unlimited Release
Printed October 2010

Determination and Optimization of Spatial Samples for Distributed Measurements

Meghan Shilling, Hy D. Tran, Xiaoming Huo, Heeyong Kim

Prepared by
Sandia National Laboratories
Albuquerque, New Mexico 87185 and Livermore, California 94550

Sandia National Laboratories is a multi-program laboratory managed and operated by Sandia Corporation, a wholly owned subsidiary of Lockheed Martin Corporation, for the U.S. Department of Energy's National Nuclear Security Administration under contract DE-AC04-94AL85000.

Issued by Sandia National Laboratories, operated for the United States Department of Energy by Sandia Corporation.

Available to DOE and DOE contractors from
U.S. Department of Energy
Office of Scientific and Technical Information
P.O. Box 62
Oak Ridge, TN 37831

Telephone: (865) 576-8401
Facsimile: (865) 576-5728
E-Mail: reports@adonis.osti.gov
Online ordering: http://www.osti.gov/bridge

Available to the public from
U.S. Department of Commerce
National Technical Information Service
5285 Port Royal Rd.
Springfield, VA 22161

Telephone: (800) 553-6847
Facsimile: (703) 605-6900
E-Mail: orders@ntis.fedworld.gov
Online order: http://www.ntis.gov/help/ordermethods.asp?loc=7-4-0#online

SAND2010-7333
Unlimited Release
Printed October 2010

Determination and Optimization of Spatial Samples for Distributed Measurements

Meghan Shilling and Hy Tran
Primary Standards Laboratory
Sandia National Laboratories
P.O. Box 5800
Albuquerque, New Mexico 87185-MS0665

Xiaoming Huo and Heeyong Kim
School of Industrial and Systems Engineering
Georgia Institute of Technology
765 Ferst Drive, NW
Atlanta, GA 30332-0205

Abstract

There are no accepted standards for determining how many measurements to take during part inspection or where to take them, or for assessing confidence in the evaluation of acceptance based on these measurements. The goal of this work was to develop a standard method for determining the number of measurements, together with the spatial distribution of measurements and the associated risks for false acceptance and false rejection. Two paths have been taken to create a standard method for selecting sampling points. A wavelet-based model has been developed to select measurement points and to determine confidence in the measurement after the points are taken. An adaptive sampling strategy has been studied to determine implementation feasibility on commercial measurement equipment. Results using both real and simulated data are presented for each of the paths.

Acknowledgements

This work is a product of the Laboratory Directed Research and Development program at Sandia National Laboratories. Sandia is a multiprogram laboratory operated by Sandia Corporation, a Lockheed Martin Company, for the United States Department of Energy's National Nuclear Security Administration under contract DE-AC04-94AL85000.

Table of Contents

List of Figures

1 Executive Summary

When measuring or inspecting products for acceptance, inspection criteria typically require a single value; however, this single value is not representative of the way that the measurement is taken. For example, a form specification on a machined part, such as circularity or roundness, gives a single value for maximum acceptable deviation of the radius of a part. The inspection of this radius, however, will typically require multiple measurements. There are no accepted standards for determining how many measurements to take or where to take them, or for assessing confidence in the evaluation of acceptance based on these measurements. The goal of this work was to develop a standard method for determining the number of measurements, together with the spatial distribution of measurements and the associated risks for false acceptance (accepting a part which does not conform to specifications) and false rejection (rejecting a part which is, in fact, conforming). The focus of this work is dimensional inspection; however, the fundamental method developed should easily be extensible to other measurement domains which have spatial distribution, such as temperature distribution.

Two paths have been taken to create a standard method for selecting sampling points. The first focuses on applying orthogonal transforms, such as the discrete wavelet transform (DWT), to compute model-based geometry and determine optimal sampling locations. The inverse transform is then applied to reconstruct measured geometry, and compare with model geometry for acceptance. Confidence bounds are computed. This provides a mathematical basis for assigning measurement uncertainty and risk for complex measurements.

Based on the results from wavelet-based method, we have determined that the mathematics for a priori selection of confidence bounds is not generally solvable. Therefore, we have also chosen to also investigate the feasibility of using an iterative method (such as adaptive sampling) to generate a measurement with a desired level of measurement uncertainty and confidence.

Simulated and real results are presented for both methodologies.

2 Motivation

To ensure the quality of a manufactured part, one needs to decide whether the part meets its design specifications. Dimensional inspection is used to measure the geometric form of a part. By comparing the measured geometry with the design specifications, the form error can be calculated. Acceptance decisions are made based on comparing the error to the specified tolerance.

Each part feature, such as straightness, can be measured in a number of different ways. Coordinate Measuring Machines (CMMs) have been widely used in modern manufacturing [1],[2]. According to Bosch [3], up to that time, fifteen billion US dollars had been spent for CMMs, with worldwide annual sales being in the range of one billion, and two hundred thousand CMMs being used by a wide range of manufacturers. More recently, annual metrology sales (including CMMs) worldwide were estimated to be around 10 billion US dollars.[†]

CMMs typically use a touch probe to collect measurements of the part surface at discrete points. A CMM functions in two basic modes: point-by-point (in which the probe touches the surface once per sampling point) and scanning (in which the probe does not leave the surface). The inspector can determine the number and location of the measurement points. Most CMMs can do point-by-point sampling; only a small proportion of CMMs can implement scanning sampling. There are two intertwined problems:

- How can you select the positions of the sample points, so that maximum part information can be obtained from a limited number of points?
- Given the limited number of measurement points, how can you construct a confidence band for the examined geometric feature and assess the form error, so that it can be reliably decided whether the part is acceptable?

For the first problem, sampling strategies for CMM measurements have been extensively studied. These strategies can be broken into three categories: “blind” sampling strageies,

[†] During 2005-2006, Hexagon Metrology believes they have 15% market share (http://www.hexagon.se/), with an annual sale of around 1.7 billion US dollars.

adaptive sampling strategies, and manufacturing-based sampling strategies [4]. Blind sampling strategies, the most commonly used, pre-determine sets of sampling points that remain the same regardless of the specific characteristics of the manufactured part. Some of the commonly used methods to pre-determine measurement points are: uniform, random, and stratified sampling [5]. Three other sampling strategies, Hammersley, Halton-Zaremba, and aligned systematic have been tested at various sample sizes [6]. Lee et al. [7] conclude that using a Hammersley sequence, when compared to a uniform sampling strategy, allows a nearly quadratic reduction in the number of samples needed while maintaining the same level of accuracy.

Adaptive sampling strategies have also been proposed [8]. These strategies start with a small set of pre-determined points. Criteria are established to determine when the set of sample points is sufficient (no additional points need to be measured). Based on the initial points, certain areas are selected for further evaluation, based the established criteria. These additional points are the evaluated with respect to the stopping criteria. This procedure continues until the sampled points meet the criteria. Application of adaptive sampling is limited, in part because programming methods for typical CMMs can make this type of iterative measurement difficult to implement. Additionally, concerns with the collisions between the probe and the workpiece or fixturing have prevented implementation of adaptive sampling [4]. We consider the feasibility of programming a CMM to implement an adaptive sampling strategy in Section 4.

The third type of sampling, manufacturing-based, considers the manufacturing signature, or typical geometric deviation pattern, left by the manufacturing process on the part. This type of sampling requires that the manufacturing signature be known, either through modeling of the machining process through evaluation of a number or surfaces [9] or through analysis of raw data from a set of densely inspected parts [4]. This type of sampling has significant drawbacks because it requires significant prior knowledge of either the machine tool used to make the part (modeling method) or of the manufactured part (raw data method).

Hocken et al. [10] provides a survey of work done in determining sampling strategies for a variety of two and three dimensional shapes. They conclude that current inspection techniques result in an under-sampling of geometric features on parts with unknown form and measurement

errors. They also make a case for the use of intelligent decision systems or procedures for choosing measurement strategies, because best choice is often counter-intuitive.

Existing studies do not take advantage of the smoothness property of the surface, our proposed statistical model which is used in combination with orthogonal transforms (Method 1) takes advantage of this property.

For the second question, there have been extensive studies for form error assessment using CMM measurements. Two most popular methods are the minimum zone (MZ) method and the orthogonal least squares (OLS) method [11, 12]. The MZ method finds the maximum inscribing and minimum circumscribing features that bound all the CMM data and uses the orthogonal width to estimate the form error. The OLS method fits an ideal feature to CMM data by minimizing the sum of squared orthogonal residuals and uses the range of the resulting orthogonal residuals to estimate the form error. Recently, Xia et al. [13] proposed the Gaussian process model, in which a sequence of CMM measurements are decomposed into three components: global trend, spatially correlated systematic errors, and spatially uncorrelated random errors. Based on the Gaussian process models of both systematic and random errors, a part surface is predicted, and the form error is subsequently estimated by finding the maximum inscribing and minimum circumscribing geometry that bounds all points on the predicted surface.

3 Wavelet-based Method

We propose a wavelet-based model, taking advantage of the fact that the Lipschitz regularity, a measure of smoothness, holds for the surface. Based on the wavelet framework, the proposed model gives the optimal sampling positions with respect to the model used. After obtaining the measurements, one can then construct confidence bands and estimate form error using a proposed wavelet-based random curve interpolating scheme. The proposed method is validated using both synthetic and real coordinate measuring machine data concerning straightness. The comparison with other existing methods demonstrates its effectiveness in generating a confidence bound.

3.1 Introduction

We propose a wavelet-based method to deal with the two questions mentioned above. Through the proposed method, one can construct confidence bands, assess form error, and determine the sampling positions. Differing from the existing literature, we use data to motivate our model, instead of imposing a model to the data. It turns out that a particular model that is based on the wavelet transform is an ideal model for CMM measurements.

We start with studying the properties of the CMM measurements. It is found that the Lipschitz regularity holds for the CMM data, when the scanning method is used. It is also known that some specially designed wavelets are Lipschitz, and the wavelet coefficients of a Lipschitz curve decay exponentially as a function of the scale index. Combining these two, we introduce a statistical model for the CMM data. Based on this statistical model, one can construct a confidence band. Furthermore, form error assessment can be carried out. The proposed model also provides a way to determine the sampling positions. It turns out that for this model, the optimal sampling positions should be the maximum point of the scaling functions in the corresponding wavelet transform. We use both real and synthetic data to test the proposed model. The Lipschitz regularity of the measured surface is justified by considering the surface properties resulting from typical machining operations.

We describe a hypothetical scenario, to demonstrate how to adopt our model in engineering application. Suppose there are many surfaces to be examined for flatness (via straightness). We confirm the Lipschitz property of surfaces made by the manufacturing process (see 3.2.1), by

taking dense data on a sample part, and studying the smoothness property of these surfaces via the wavelet transform method that will be described later. When the Lipschitz property is confirmed, one can adopt our model to construct a confidence band, assess the form error, and most importantly, determine the optimal positions where a small number of samples need to be taken. By reducing the sampling positions, the entire inspection process is expedited. The smoothness property of the surface (across multiple parts) will not change unless the manufacturing process is changed (see 3.2.1).

In section 3.2, the formulation of the CMM data is presented; the measurements are statistically modeled via wavelet decomposition. Based on such a model, in section 3.3, we propose a wavelet-based method to construct a confidence band for the measurements, to assess form error, and to determine the optimal sampling positions. Our method is validated with real and synthetic data in section 3.4 and section 3.5, respectively. In section 3.6, some justification and future extension of our method are discussed. Finally, we present conclusions concerning this wavelet-based method in section 0.

3.2 Background and Formulation

The formulation for this method is based on common problems encountered when measuring a continuous surface with discrete points. As an example, Figure 1 contains two sub-figures, which are real measurements taken in a CMM facility at Sandia National Laboratories in New Mexico. The data are taken on the same surface, along a straight line, with an objective to measure the straightness. They are obtained in two approaches: a point-by-point scheme and a scanning scheme. In both sub-figures, the x-axis is along the surface, while the vertical axis is normal to the surface.

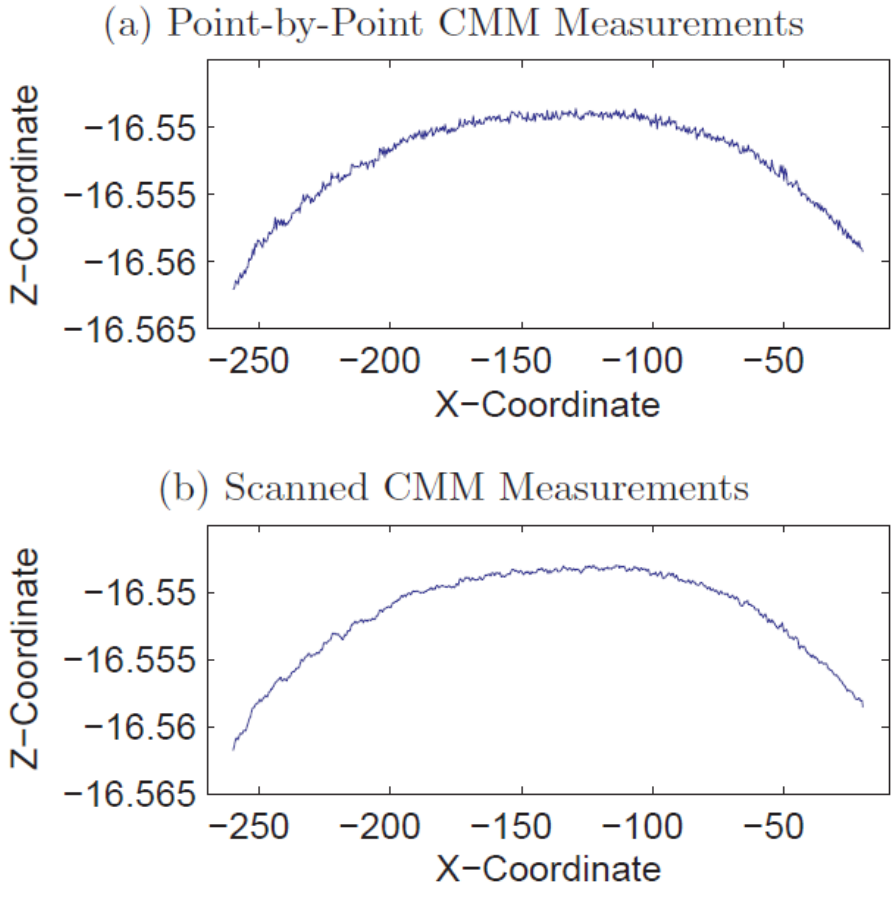

Figure 1: Two real sequences of CMM measurements. The lengths are 512 and 1201, respectively. Only the x and z-coordinates are of interest (because we consider the straightness of the line). The unit for both axes is 10^{-3} meter.

For this method, we first consider the mathematical property of the surface, on which the CMM data are taken. It is observed that if one takes a straight line on the surface, the resulting curve is uniformly Lipschitz. Because of such a property, the wavelet orthonormal bases can be utilized to create a model for the CMM data. The statistical model imposes statistical distributions on the wavelet coefficients. In our approach, the adoption of wavelets is a consequence, instead of a pre-assumption. We describe details in the following subsections.

The Lipschitz property is reviewed in 3.2.1; we also discuss justification of such an assumption on part surfaces. The wavelets basis functions and the properties of wavelet coefficients for Lipschitz functions are presented in 3.2.2 and 3.2.3, respectively. A statistical model for CMM measurements (which is taken from a Lipschitz function) is presented in 3.2.4. Sections 3.2.1 through 3.2.3 are based on continuum. Due to the nature of CMM measurements, 3.2.4 is written for discrete data.

3.2.1 Lipschitz Regularity and Justification Related to Part Surface

Recall a function $f(\bullet)$ is pointwise Lipschitz γ $(\gamma > 0)$ [14] at point *x* if there exists a constant *K*> 0 and a polynomial $p_x(t)$ in the neighborhood of *x*, of degree $\lfloor\gamma\rfloor$ (i.e., the largest integer no larger than γ) such that

$$\forall t \in \mathbb{R}, \quad \left| f(t) - p_x(t) \right| \le K \left| t - x \right|^{\gamma} \qquad \text{Equation 1}$$

A function is uniformly Lipschitz γ over [*a, b*] ($a \le b$) if for all $x \in [a,b]$, there is a constant *K* (that is independent of *x*) such that Equation 1 holds. The Lipschitz regularity of a function *f* is the supreme of γ such that *f* is uniformly Lipschitz γ. Lipschitz regularity can measure the smoothness of *f.* The essence of Lipschitz regularity is how *f* can be locally approximated by a polynomial function—whose degree is a natural indicator of the smoothness.

The CMM is often utilized to measure the straightness of a machined surface. The act of machining intuitively leads to a surface that is locally polynomial. Below, we discuss physical justification on this assumption. A test on real data will be presented in section 3.4. Manufacturing errors in machining are attributed to geometrical errors in the machine (such as quasi-static errors due to machine error motions, thermally induced geometrical errors) [15]. In addition, cutter/material interactions will also produce surface roughness and finish imperfections [16]. Surface roughness and finish in machining operations, such as milling, are typically on the order of 0.8 to 6.3 micrometer roughness average [17]. Another contributor to form error is tool/cutter deflections. This “copying” error [18] can be modeled as a linear spring-mass-damper system [19] and can be minimized with proper selection of machining parameters [20]. Typical tolerances specified on machined parts are much larger than the surface roughness and finish [21], for example, on the order of 100 micrometer for geometry fabricated by end-milling. In typical machining practice and measurement equipment practice, the machine geometrical errors are mapped at discrete points, with linear interpolation between the mapped points [10]. This makes the machine geometry follow a piecewise linear path, which is also piecewise polynomial.

3.2.2 Orthonormal Wavelets Basis

We now review some basics of wavelets. For f(x), its wavelet decomposition has a form:

$$f(x) = \sum_{j \in I_L} \alpha_j \phi_j(x) + \sum_{i>L} \sum_{j \in I_L} \beta_{ij} \psi_{ij}(x) \qquad \text{Equation 2}$$

where $\phi_j(x)$ are scaling functions at the coarsest scale, $\psi_{ij}(x)$ are wavelet functions, L is the coarsest scale, I_L is the set of location indices at the coarsest scale while I_i is the set of location indices at scale i, finally, i and j are the scale and location indices, respectively. Note that $\phi_j(x)$ and $\psi_{ij}(x)$ can be derived by shifting and scaling: $\phi_j(x) = \phi(x - j \bullet c)$ and $\psi_{ij}(x) = \psi\left(2^{i-L} \cdot x - j \cdot c\right) \cdot 2^{\frac{1}{2}(i-L)}$. Mostly, we choose ϕ and ψ with finite support; e.g., the Daubechies' wavelets. It is known that if ψ has p vanishing moments, then ϕ and ψ are roughly Lipschitz γ with $\gamma \approx 0.2p$. We refer to Chapter 7 of [14] for more details. We will use the Lipschitz condition of Daubechies' wavelets. Moreover, we will need the following result.

Theorem 1: If ψ is uniformly Lipschitz γ with constant K, then $\psi_{ij}(i > l)$ is also Lipschitz γ with constant $K \cdot 2^{(i-L)\left(\gamma + \frac{1}{2}\right)}$

.

Proof: Recall we have

$$\left|\psi(t) - p_x(t)\right| \le K \left|t - x\right|^{\gamma}$$

where $p_x(t)$ is a polynomial given in Equation 1. One can easily verify the following:

$$\left|2^{\frac{1}{2}(i-L)} \psi\left(2^{i-L} \cdot t\right) - p_{x \cdot 2^{(i-L)}}\left(2^{i-L} \cdot t\right) \cdot 2^{\frac{1}{2}(i-L)}\right| \le K \cdot 2^{(i-L)\left(\gamma + \frac{1}{2}\right)} \left|t - x\right|^{\gamma}$$

The above is equivalent to the fact that ψ_{ij} is Lipschitz γ with $2^{(i-L)\left(\gamma + \frac{1}{2}\right)} K$.

3.2.3 Properties of Wavelets Coefficients

We review an important property of wavelet coefficients. This property is the foundation of our statistical model. If function f is smooth, then the wavelet coefficients β_{ij} decay exponentially as a function of the scale: For example, if f is uniformly Lipschitz γ over [0, 1], then we have $\beta_{ij} < A \cdot 2^{-\sigma i}$, where A is a constant and $\sigma = \gamma + \frac{1}{2}$ ([14] Section 6.1, Theorem 6.3). We utilize the above property to construct a system, which can generate Lipschitz γ curves. Note that Equation 2 involves infinite scales. In practice, we do not need to consider a function with

infinite fine scales—we sacrifice some mathematical rigor here. We consider a truncated case: for $L' > L$, we consider

$$f(x) = \sum_{j \in I_L} \alpha_j \phi_j(x) + \sum_{i=L+1}^{L'} \sum_{j \in Ii} \beta_{ij} \psi_{ij}(x) \qquad \text{Equation 3}$$

where L' determines how well (i.e., up to which fine scale in the multiresolution analysis) the experimenter wants our model to approximate the true curve. Note that for fixed $i \in \{L+1, L+2, ..., L'\}$, and fixed x, $\sum_{j \in I_i} \psi_{ij}(x)$ only has finite number of nonzero terms. In particular, if we consider Daubechies' wavelets with p vanishing moments, the number of nonzero terms is $2p + 1$. We will need the following property.

Theorem 2: In Equation 3, if we impose $|\beta_{ij}| \le A \cdot 2^{-\left(\gamma+\frac{1}{2}\right)(i-L)}$ and ψ, ϕ are Lipschitz γ with constant K, then *f(x)* is Lipschitz γ with constant that is determined by K, A, $L' - L$, and α_j's.

Proof: Similar to the proof for Theorem 1, we can show that:

1. $\sum_{j \in I_L} \alpha_j \phi_j(x)$ is Lipschitz γ with constant $K \cdot \sup_k \sum_{j=k}^{k+2p} |\alpha_j|$.
2. For fixed $i \in [L+1, L']$, $\sum_{j \in I_i} \beta_{ij} \psi_{ij}(x)$ is Lipschitz γ with constant $(2p+1) \cdot K \cdot A$ (Note that we need to call Theorem 1 to establish this result.)

Overall, *f(x)* is Lipschitz γ with constant: $K \cdot \sup_k \sum_{j=k}^{k+2p} |\alpha_j| + (2p+1) \cdot K \cdot A \cdot (L - L')$.

3.2.4 Proposed Statistical Model

Taking advantage of Theorem 2, we establish the following statistical model for the CMM measurements. Recall that Equation 3 contains a model of *f(x)* in continuum. CMM measurements are always discrete. Section 2 of [13] gives a nice description on CMM data modeling; this paper adopts a similar approach. The sampling points are denoted by $S_\ell, \ell = 1, 2, ..., N$, where N is the sample size. Let Y_ℓ denote the relevant CMM measurement at S_ℓ, we assume that

$$Y_\ell = f(S_\ell) + \varepsilon_\ell, \quad 1 \le \ell \le N \qquad \text{Equation 4}$$

where $f(\cdot)$ is given in Equation 3 and ε_ℓ's are measurement errors. If in relative to $f(S_\ell)$, error ε_ℓ is negligibly small, the property of Y_ℓ's is mainly up to the underlying function *f(x)*. Our model is intended for such a situation.

Now we focus on the situation when ε_ℓ's are negligibly small and *f(x)* is Lipschitz. We adopt Daubechies' wavelets with *p* vanishing moments. Other wavelets may be chosen, as long as they satisfy the Lipschitz condition and the finite-support condition that we required. Moreover, we impose that

$$\left|\beta_{ij}\right| \le A \cdot 2^{-\left(\gamma+\frac{1}{2}\right)(i-L)} \qquad \text{Equation 5}$$

where *A* is a prescribed constant, and γ is a prescribed regularity index. The CMM measurements Y_ℓ's are given in Equation 4 with *f(x)* specified inEquation 3; i.e., we have

$$Y_\ell = f(S_\ell) + \varepsilon_\ell = \sum_{j \in I_L} \alpha_j \phi_j(S_\ell) + \sum_{i=L+1}^{L'} \sum_{j \in I_i} \beta_{ij} \psi_{ij}(S_\ell) + \varepsilon_\ell, \quad \ell = 1, 2, ..., n \qquad \text{Equation 6}$$

There is no particular restriction on α_j; hence the model can accommodate functions with various shapes.

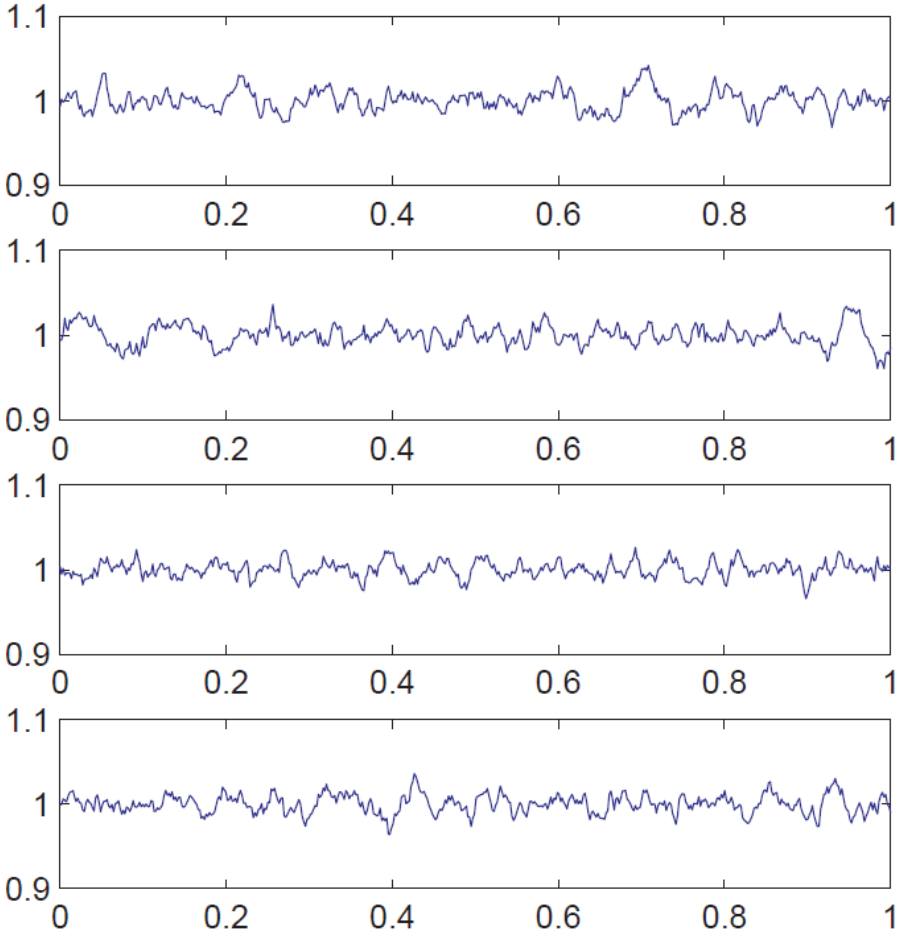

Figure 2: Four simulated Lipschitz-0.5 curves by utilizing Daubechies' symmlets.

For illustration purpose, Figure 2 presents four curves by setting $\beta_{ij} \sim \frac{1}{10} 2^{-\sigma(i-L)} \cdot N(0,1)$, where the total length of signal is $N = 2^9 = 512$ and the coarsest scale is L = 4. The Daubechies' nearly symmetric wavelets (a.k.a. Symmlets) with six vanishing moments is adopted. We choose σ =1 (correspondingly, γ =0.5). Coefficients of all scaling functions (α_j's) are set to be zero - this is why these simulated curves look flat, while the measured data in Figure 1 are not. Despite the shape (i.e., focusing on the smoothness), we find that such a curve resembles the real data that are obtained via CMMs.

The aforementioned β_{ij}'s satisfy the normal distribution, which is not strictly bounded. However, it is known that normal distribution is highly concentrated around zero. For example, it is extremely unlike to have a realization of a normally distributed random variable that is six

standard deviations away from its mean. Hence in simulation, one can treat it as a bounded random variable without much loss. The QQ plots that will be displayed in section 3.4 show that for real CMMs data, when the measurement errors are negligibly small (e.g., scanning data), the β_{ij}'s do satisfy the normal distribution.

3.3 Proposed Methods

We describe our strategy for three key problems in analyzing CMM data (with regard to straightness). Our construction of confidence bands is described in 3.3.1. When reduced sample size is pursued, an optimal sampling strategy is derived in 3.3.2. Form error assessment is studied in 3.3.3.

3.3.1 Confidence Band

To construct a confidence band, we first specify the baseline (denoted by *b(x)*) of the band. When the half-width (denoted by *w*) is given, the confidence band is simply $b(x) \pm w : \{(x, y) : b(x) - w \le y \le b(x) + w\}$. We first describe our methods of specifying *b(x)* in 3.3.1.1. The *w* is determined in 3.3.1.2. How to use the constructed confidence *b* and towards the part acceptance is discussed in 3.3.1.3. Our purpose is to decide the straightness, hence the assumption on constant bandwidth (*w*) is justifiable.

3.3.1.1 Baseline

Recall the CMM model in Equation 6. Nearly all wavelet transforms are based on equally spaced samples. Without loss of generality, here we assume that $S_\ell = \ell / N, \ell = 1, 2, ..., N$. (Note when S_ℓ's are not equally spaced, as long as *N* is large and the sampling is dense everywhere, one may adopt an interpolation strategy to transform them into equally spaced samples.) Estimating the baseline is essentially a smoothing operation. So we assume standard properties on ε_ℓ's, e.g., they are white noise. Note that we are interested in the case when ε_ℓ's are very small in relative to the first two terms in Equation 6. The deviation of ε_ℓ's from the above assumption will not be devastating. We describe two approaches to specify *b(x)*.

- We can simply use the measurement sequence as the baseline. The disadvantage is that the measured curve can be noisy. The justification of this approach is that for each position, the observed is a point estimate of *b(x)* at the corresponding location.

- We first carry out a wavelet transform of the measured data. Suppose that the wavelet coefficients are $\left\{\hat{\alpha}_j, \hat{\beta}_{ij}, i = L+1, ..., L'\right\}$. The hat indicates that they are computed from the observations. We then set $\beta_{ij} = 0$ for $i > L_0$, where $L+1 \le L_0 \le L'$. Such an approach is identical with the wavelet shrinkage [22] method, which has many nice statistical properties. We then apply inverse wavelet transform to the shrunken coefficients. The result is our baseline estimate *b(x)*.

In our numerical study, we adopt the latter approach, because it renders a smoother baseline.

3.3.1.2 Width of the Confidence Band

To determine *w*, there are at least two approaches. The first one is conservative; it furnishes a wider band. The second one is more accurate, given that the assumed statistical model is close to the reality.

- Recall that for any *x*, ignoring the small error term, we have

$$f(x) = \sum_{j \in I_L} \alpha_j \phi_j(x) + \sum_{i>L} \sum_{j \in I_i} \beta_{ij} \psi_{ij}(x)$$

We treat $\sum_{j \in I_L} \alpha_j \phi_j(x)$ as the baseline; because this part is not random. The random component (denoted by *u(x)*) becomes

$$u(x) = f(x) - \sum_{j \in I_L} \alpha_j \phi_j(x)$$

By design, we have $\left|\beta_{ij}\right| \le A \cdot 2^{-\sigma i}$, which leads to

$$\left|u(x)\right| \le \sum_{i>L} \sum_{j \in I_i} \left|\psi_{ij}(x)\right| \cdot A \cdot 2^{-\sigma i}$$

Note that $\psi_{ij}(x)$ is a wavelet function, which is a result of scaling and shifting of a standard (finite supported) function $\psi : \psi_{ij}(x) = 2^{i/2} \psi\left(2^i x - j \cdot c\right)$. For fixed *i*, the following should be upper bounded:

$$2^{-i/2} \sum_{j \in I_i} \left|\psi_{ij}(x)\right| = \sum_{j \in I_i} \left|\psi_{ij}\left(2^i x - j\right)\right| < \text{constant} = C_1$$

Hence as long as $\sigma > 1/2$, we have that

$$\left|u(x)\right| \le C_1 \sum_{i>L} 2^{i/2} \cdot A \cdot 2^{-\sigma i} = C_1 \cdot A \cdot \sum_{i>L} 2^{-i(\sigma - 1/2)} < \text{constant}$$

The above also points out a way to compute the upper bound.

- The aforementioned gives the worst-case bound. We can derive a more accurate bound via simulation. Recall that

$$u(x) = \sum_{i>L} \sum_{j \in I_i} \beta_{ij} \psi_{ij}(x)$$

For fixed x, $\psi_{ij}(x)$'s are fixed. We choose $\beta_{ij} \sim A \cdot 2^{-\sigma(i-L)} \cdot N(0,1)$, where L is the coarsest scale and $i>L$, A is fixed. Let $\|u(x)\|_\infty$ denote the supreme of $|u(x)| : \|u(x)\|_\infty = \sup|u(x)|$. Note $\|u(x)\|_\infty$ is a random number. Its percentiles (e.g., the 99th percentile) can be estimated via simulation.

In simulation study, it occurs that the bounds in the former method is usually 2 or more orders of magnitude larger than the counterpart that is given by the latter method. This indicates that the former method is too conservative, and contains too many zero-probability events. Furthermore, in our simulation study with real data sets, in almost all the time we observed that the β_{ij}'s at fixed i behave like normally distributed random variables, referring to section 3.4 and Figure 7. Hence in our simulation, we choose the latter.

3.3.1.3 Use of Confidence Bands

Once a confidence band is constructed, one can make part acceptance decision accordingly. Acceptance of parts is based on an agreement between the producer and the consumer. The consumer has a functional need for the nominal measured quantity; where if the part deviates too far from the nominal value, the part will not function. With simple acceptance [23], if the measurement falls outside the tolerance zone, the part is rejected. Frequently, the customer and producer will agree that the measurement equipment uncertainty must be some ratio smaller than the tolerance zone, in order to use simple acceptance. Another frequently used standard [24] incorporates a decision rule based on the probability of false acceptance (probability that a part measured as acceptable is actually non-conforming is < 2%). The derived confidence band is compared with the tolerance specification in order to determine the acceptance.

The tolerance is also often specified by consumers as form error. Given a confidence band, one can estimate the form error using, e.g., the minimum zone approach. The result is compared with

the tolerance level that is given by the consumer and a decision can be made accordingly. A potential limitation of this approach is discussed in 3.3.3.

3.3.2 Optimal Sampling Positions

We now consider how to determine the optimal sampling positions for a new surface that needs to be examined. We will address this problem in two steps. Firstly, we suppose that a few samples have been taken, and we need to estimate the baseline. We introduce our interpolating scheme, which adopts the minimum energy principle. A closed-form solution is presented (3.3.2.2). Secondly, based on the result from the first step, we consider what will be the optimal sampling positions. Under our framework, we argue that the optimal sampling positions should be chosen at the positions where the scaling functions take the maxima (Section 3.2.3).

3.3.2.1 Problem Description and Notations

Recall in 3.2.4 that the CMM measurements are modeled as $Y_\ell = f\left(S_\ell\right), 1 \le L \le N$, where S_ℓ is a sampling position on which a discrete wavelet transform is based (we assume that $\varepsilon_\ell \approx 0$). From this point, we let $\left\{S_\ell\right\}_{l=1}^{N}$ denote a dense enough set of measurements (i.e., N is large enough), while a subset of $\left\{S_\ell\right\}_{l=1}^{N}$ (i.e., much smaller number of samples) is denoted by c where $n \ll N$; recalling that we assigned $S_\ell = \frac{\ell}{N}$ in 3.3.1.1, so $\left\{s_\ell\right\}$ is a subset of $\left\{\frac{1}{N}, \frac{2}{N}, ..., 1\right\}$. The objective is to find the optimal positions of $\left\{s_\ell\right\}$. According to Equation 6 we have a system of linear equations for the measurements at $\left\{s_\ell\right\}$:

$$y_\ell = f\left(s_\ell\right) = \sum_{j \in I_L} \alpha_j \phi_j\left(s_\ell\right) + \sum_{i=L+1}^{L'} \sum_{j \in I_i} \beta_{ij} \psi_{ij}\left(s_\ell\right), \quad \ell = 1, 2, ..., n \qquad \text{Equation 7}$$

Note the error ε_ℓ is tentatively left out; because we focus on the true surface at this moment. If we consider the dense set of measurements at $\left\{S_\ell\right\}$, we have a complete system of equations:

$$Y_\ell = f\left(\ell / N\right) = \sum_{j \in I_L} \alpha_j \phi_j\left(\ell / N\right) + \sum_{i=L+1}^{L'} \sum_{j \in I_i} \beta_{ij} \psi_{ij}\left(\ell / N\right), \quad \ell = 1, 2, ..., N \qquad \text{Equation 8}$$

Note that the equations inEquation 7 is a subset of equations inEquation 8. We introduce notations that will facilitate future discussion. Let $Y = \left(f\left(1/N\right), f\left(2/N\right), ..., f\left(1\right)\right)^T$,

$\alpha = \left(\alpha_1, \alpha_2, ..., \alpha_{2^L}\right)^T$, $\beta = \left(\beta_{ij}\right)^T$ - i.e., β is a column vector that contains all β_{ij}'s. Let $\mathbf{\Phi}_1 = \left(\phi_j\left(\ell / N\right)\right)_{\ell j}$ and $\mathbf{\Phi}_2 = \left(\psi_{ij}\left(\ell / N\right)\right)_{\ell, ij}$ matrix $\mathbf{\Phi}_2$ contains all values $\psi_{ij}\left(\ell / N\right)$ in Equation 8. The system in Equation 8 can be rewritten as

$$Y = \mathbf{\Phi}_1 \alpha + \mathbf{\Phi}_2 \beta \qquad \text{Equation 9}$$

Let $y = \left(y_1, y_2, ...y_n\right)^T$; i.e., y is a subset of Y, consisting of the measurements at $\left\{s_\ell\right\}_{l=1}^n$. We use y^c to denote the complement of y within Y. Let Φ_1 and Φ_2 denote the subset of rows of $\mathbf{\Phi}_1$ and $\mathbf{\Phi}_2$ whose membership is consistent with $\left\{s_1, s_2, ..., s_n\right\}$ being a subset of $\left\{1/N, 2/N, ..., N\right\}$. The equations Equation 7 is equivalent to the following:

$$y = \Phi_1 \alpha + \Phi_2 \beta \qquad \text{Equation 10}$$

Moreover, let Φ_1^c and Φ_2^c denote the matrices made by the remaining rows of $\mathbf{\Phi}_1$ and $\mathbf{\Phi}_2$ however not included in Φ_1 and Φ_2, respectively. The complete system in Equation 9 (or Equation 8) can be written as follows:

$$\begin{pmatrix} y \\ y^c \end{pmatrix} = \begin{pmatrix} \Phi_1 & \Phi_2 \\ \Phi_1^c & \Phi_2^c \end{pmatrix} \begin{pmatrix} \alpha \\ \beta \end{pmatrix} \qquad \text{Equation 11}$$

3.3.2.2 Wavelet-Based Random Curve Interpolating Algorithm

In this section, we propose an interpolating algorithm which can be used to estimate the baseline when only a small number of measurements are available (i.e., when only the measurements at $\left\{s_\ell\right\}_{l=1}^n$, not at $\left\{S_\ell\right\}_{l=1}^N$, are available.). In Equation 10, suppose y and β are known. The only unknown variable is α, which satisfies $\Phi_1 \alpha = y - \Phi_2 \beta$. The minimum ℓ^2 norm solution for α corresponds to the following optimization problem:

$$\begin{aligned} &\min_{\alpha} \quad \|\alpha\|_2^2 \\ &\text{subject to} \quad \Phi_1 \alpha = y - \Phi_2 \beta \end{aligned} \qquad \text{Equation 12}$$

We have the following lemma for the solution to the above problem.

Lemma 1 Equation 12 is a quadratic programming problem, which has the closed-form solution:

$$\alpha = \Phi_1^T \left(\Phi_1 \Phi_1^T\right)^{-1} \left(y - \Phi_2 \beta\right) \qquad \text{Equation 13}$$

The proof has been relegated to Appendix A.

Using Lemma 1, we propose an interpolating algorithm as follows (Note *y* is available):

1. Generate β such that each β_{ij} satisfies Equation 5. This ensures the Lipschitz property. (In order to generate β_{ij}, parameters *A* and σ need to be specified. Recall that we first take dense measurements (i.e., $\{S_\ell\}_{l=1}^{N}$) from a few parts to ensure Lipschitz property. The parameters *A* and σ can be estimated from the measurements at $\{S_\ell\}_{l=1}^{N}$. Estimation of A and σ from such measurements will be described in 3.4.2.)
2. Apply Lemma 1 to obtain α. The interpolated function at the dense set of sampling positions (i.e., $\ell / N, \ell = 1, 2, ..., N$) is obtained by Equation 9.

The above method will be called minimum energy interpolation. Note when $n \ll N$, one should let the aforementioned algorithm substitute the method in 3.3.1.1. By letting $N \to \infty$, one interpolates *f(x)* nearly everywhere.

We justify the adoption of minimum energy interpolation through the following two arguments.

- We first use illustration to establish an intuition. To do so, we find an α that satisfiesEquation 10, however it is not required to be a solution inEquation 12. Figure 3 plots a minimum energy interpolating curve in black, together with two other non-minimum-energy random interpolating curves (in red and green). It is observed that minimum energy interpolating curves are closer to observations in metrology.
- Recall that in the wavelet decomposition, the coefficients of scaling functions (i.e., α) reflect the trend, while the coefficient of wavelets (i.e., β) represent the regularity (or smoothness). To ensure that the underlying function *f(·)* is Lipschitz, one only needs to impose condition Equation 5 on β. If the underlying shape is a straight line, we should have $\alpha = 0$. Recall that we examine the straightness on a surface, which leads to a small value of $\|\alpha\|_2$. (If the underlying target shape is not a straight line—e.g., roundness—then the geometric shape needs to be removed from the data, before applying the aforementioned minimum energy principle.)

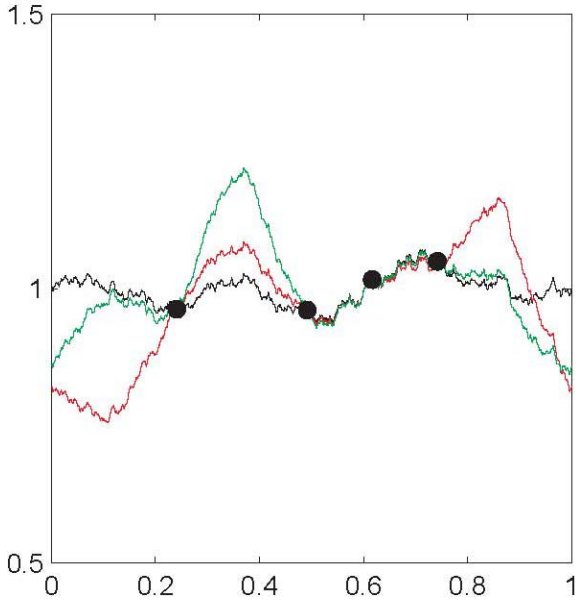

Figure 3: Non-minimum interpolating random curves (red and green ones) versus the minimum energy interpolating random curve (in black).

3.3.2.3 Optimal Sampling Positions

In this section, we consider the optimal sampling positions for $\{s_\ell\}_{l=1}^{n}$ We conclude that the optimal sampling strategy (under our model) is the one that maximizes the singular values of matrix Φ_1. Maximizing singular values of Φ_1 (via choosing different subset of rows of Φ_1) is a hard numerical problem. We introduce a heuristic approach instead.

Recall that the following denotes the complete matrix associated with the discrete wavelet transform and it is orthogonal:

$$\begin{pmatrix} \Phi_1 & \Phi_2 \\ \Phi_1^c & \Phi_2^c \end{pmatrix} \qquad \text{Equation 14}$$

Moreover, we suppose that the true surface at the sampling positions are $y = \Phi_1\alpha_0 + \Phi_2\beta_0$, i.e., α_0 and β_0 are the wavelet coefficients of the true surface. Recall in 3.3.2.2 where the minimum energy interpolating algorithm is applied, one needs to generate β. Let $\tilde{\beta}$ denote such a generated β. Recall we have $y = \Phi_1\alpha + \Phi_2\tilde{\beta}$. From Lemma 1 we have

$$\alpha = \Phi_1^T \left(\Phi_1 \Phi_1^T\right)^{-1} \left(y - \Phi_2 \tilde{\beta}\right)$$
$$\alpha = \Phi_1^T \left(\Phi_1 \Phi_1^T\right)^{-1} \left(\Phi_1 \alpha_0 + \Phi_2 \beta_0 - \Phi_2 \tilde{\beta}\right)$$
$$\alpha = \Phi_1^T \left(\Phi_1 \Phi_1^T\right)^{-1} \Phi_1 \alpha_0 + \Phi_1^T \left(\Phi_1 \Phi_1^T\right)^{-1} \Phi_2 \left(\beta_0 - \tilde{\beta}\right)$$

Let $y^c = \Phi_1^c \alpha + \Phi_2^c \tilde{\beta}$. Substituting the above α, we have

$$y^c = \Phi_1^c \Phi_1^T \left(\Phi_1 \Phi_1^T\right)^{-1} \Phi_1 \alpha_0 + \Phi_1^c \Phi_1^T \left(\Phi_1 \Phi_1^T\right)^{-1} \Phi_2 \left(\beta_0 - \tilde{\beta}\right) + \Phi_2^c \tilde{\beta}$$
$$y^c = \Phi_1^c \Phi_1^T \left(\Phi_1 \Phi_1^T\right)^{-1} \Phi_1 \alpha_0 - \Phi_2^c \Phi_2 \left(\Phi_1 \Phi_1^T\right)^{-1} \Phi_2 \left(\beta_0 - \tilde{\beta}\right) + \Phi_2^c \tilde{\beta}$$

The second equation above is based on the following:

$$0 = \begin{pmatrix} \Phi_1^c & \Phi_2^c \end{pmatrix} \begin{pmatrix} \Phi_1^T \\ \Phi_2^T \end{pmatrix} = \Phi_1^c \Phi_1^T + \Phi_2^c \Phi_2^T$$

The above is true because the matrix in Equation 14 is orthogonal. In addition, we have the difference between the interpolated and the truth as

$$y^c - \left(\Phi_1^c \alpha_0 + \Phi_2^c \beta_0\right) = \Phi_1^c \left[\Phi_1^T \left(\Phi_1 \Phi_1^T\right)^{-1} \Phi_1 - I\right] \alpha_0 + \Phi_2^c \left[\Phi_2^T \left(\Phi_1 \Phi_1^T\right)^{-1} \Phi_2 - I\right] \left(\tilde{\beta} - \beta_0\right)$$

We consider the quantity $\left\| y^c - \left(\Phi_1^c \alpha_0 + \Phi_2^c \beta_0\right) \right\|_2^2$, which is the norm of the above difference. It will be desirable if this quantity is small. Given the above equation, recalling $n \ll N$, matrix $\left(\Phi_1^c, \Phi_2^c\right)$ is a big proportion of the orthogonal matrix in Equation 14. Hence the value of $\left\| y^c - \left(\Phi_1^c \alpha_0 + \Phi_2^c \beta_0\right) \right\|_2^2$ is minimized when the norm of coefficients $M_1 \alpha_0$ and $M_2 \left(\tilde{\beta} - \beta_0\right)$ are minimized, where $M_1 = \Phi_1^T \left(\Phi_1 \Phi_1^T\right)^{-1} \Phi_1 - I$ and $M_2 = \Phi_2^T \left(\Phi_1 \Phi_1^T\right)^{-1} \Phi_2 + I$. Since α_0 and $\left(\tilde{\beta} - \beta_0\right)$ are prefixed, to minimize the norm of the coefficients, we need to minimize the eigenvalues of M_1 and M_2.

M_1 is a projection matrix. The eigenvalues of M_1 are 0's and 1's. Its eigenvalues are minimized (in fact, reduces to zero matrix) when Φ_1 is of full column rank. Recall Φ_1 has 2^L columns. If the row rank of Φ_1 is *k*, the multiplicity of one in $\Phi_1^T \left(\Phi_1 \Phi_1^T\right)^{-1} \Phi_1 - I$ is $2^L - k$. Apparently, larger *k* is more desirable. The maximal possible *k* is the sample size; i.e., Φ_1 has full row rank.

It is more delicate to study the eigenvalues of M_2. Recall that $\Phi_1\Phi_1^T + \Phi_2\Phi_2^T = I$, hence $\Phi_1\Phi_1^T$ and $\Phi_2\Phi_2^T$ can be diagonalized simultaneously. The singular value decompositions of Φ_1 and Φ_2 consequently can be written as

$$\Phi_1 = UD_1V_1, \quad \Phi_2 = UD_2V_2$$

where U, V_1, and V_2 are orthogonal and D_1, D_2 are diagonal. Moreover, we must have $D_1^2 + D_2^2 + I$

We have the following:

$$M_2 = \Phi_2^T\left(\Phi_1\Phi_1^T\right)^{-1}\Phi_2 + I$$
$$M_2 = V_2^T D_2 U^T\left(UD_1^2U^T\right)^{-1}UD_2V_2 + I$$
$$M_2 = V_2^T\left(D_2D_1^{-2}D_2 + I\right)V_2$$
$$M_2 = V_2^T\left(D_1^{-2}\right)V_2$$

Hence minimizing the eigenvalues of M2 is equivalent to maximizing the eigenvalues of $\Phi_1\Phi_1^T$ which is a hard numerical question.

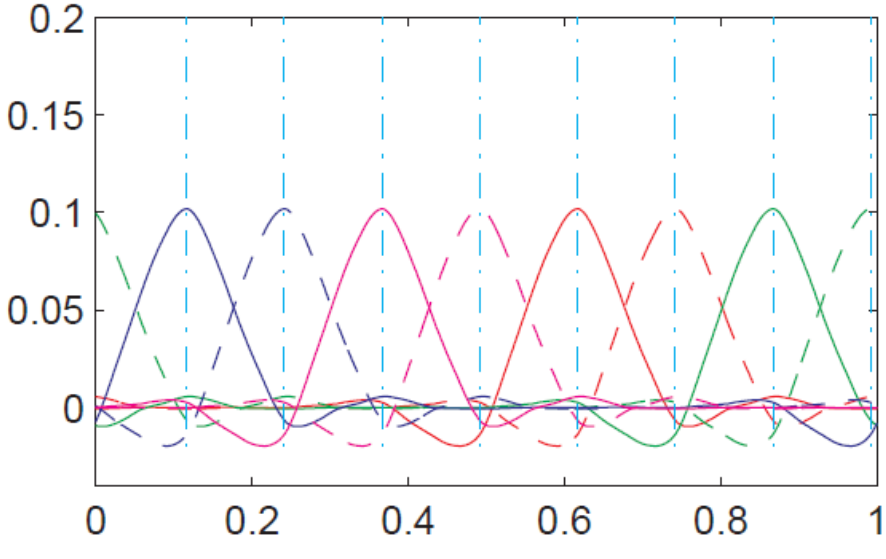

Figure 4: Scaling functions in the wavelet decomposition. The corresponding maximum positions are 0.117, 0.242, 0.367, 0.492, 0.617, 0.742, 0.867, and 0.992.

We consider a heuristic approach. Figure 4 presents eight scaling functions, corresponding to Symmlet with 6 vanishing moments at the coarsest level L = 3. Each x-coordinate corresponds to a row in the system Equation 9. Intuitively, eigenvalues of matrix $\Phi_1\Phi_1^T$ is maximized if the

matrix Φ_1 is diagonally dominated: the diagonal entries in absolute value are much bigger than off-diagonal entries. In Figure 4 this corresponds to finding locations (x-coordinate) such that one scaling function takes big value, while the other scaling functions take values close to zero at the same site. Eight of these positions are marked by dash-doted vertical lines in the figure; they are the optimal sampling positions.

3.3.3 Form Error Assessment

Tolerances are frequently specified as maximum permissible error in form. After obtaining the baseline *b(x)* and the half-width *w* of the confidence band, one can assess the form error by applying the minimum zone (MZ) method. The MZ method can find the narrowest tube that contains the confidence band; then the width of the narrowest tube is the estimate of the form error. Evidently, such approach leads to conservatism—the confidence band tends to be larger than a tube based on CMM measurement points alone. On the other hand, there has been an interest in the literature to estimate the underlying form error unbiasedly (e.g. [13]). In this section, we propose a method to estimate the form error that is consistent with this line of research. Simulations (in 3.5.2) render satisfactory results.

Recall our statistical model for the dense set of measurements:

$$Y_\ell = f\left(\ell / N\right) = \sum_{j \in I_L} \alpha_j \phi_j\left(\ell / N\right) + \sum_{i=L+1}^{L'} \sum_{j \in I_i} \beta_{ij} \psi_{ij}\left(\ell / N\right) + \varepsilon_\ell, \quad \ell = 1, 2, ..., N$$

Note that in the above equation, comparing to Equation 8, the measurement errors ε_ℓ are considered. We assume that $\left\{\frac{\ell}{N}\right\}_{\ell=1}^{N}$ are dense. Following a tradition (e.g. [13]), the 'true' form error is the outcome by applying the MZ method to $\left\{\left(\frac{\ell}{N}, Y_\ell\right)\right\}_{\ell=1}^{N}$ Our objective is to estimate this true form error unbiasedly using only a small subset of $\left\{\left(\frac{\ell}{N}, Y_\ell\right)\right\}_{\ell=1}^{N}$, i.e., using $\left\{\left(s_\ell, y_\ell\right)\right\}_{\ell=1}^{n}$ where $n \ll N$. Note that the positions of $\left\{s_\ell\right\}_{\ell=1}^{n}$ can be decided using the sampling strategy proposed in 3.3.2.3. Considering the measurement errors, the measurements at $\left\{s_\ell\right\}_{\ell=1}^{n}$ are

$$y_\ell = \sum_{j \in I_L} \alpha_j \phi_j\left(s_\ell\right) + \sum_{i=L+1}^{L'} \sum_{j \in I_i} \beta_{ij} \psi_{ij}\left(s_\ell\right) + \varepsilon_\ell, \quad \ell = 1, 2, ..., N$$

We propose the following method to estimate the form error using the measurements $\{(s_\ell, y_\ell)\}_{\ell=1}^{n}$.

1. Given $\{(s_\ell, y_\ell)\}_{\ell=1}^{n}$, we estimate the baseline sequence (denoted by $\{b(\ell/N)\}_{\ell=1}^{N}$) via the minimum energy interpolating scheme proposed in 3.3.2.2. Given $\{(s_\ell, y_\ell)\}_{\ell=1}^{n}$, after assigning $\beta_{ij} = 0$, one can compute the α as in Equation 13. Consequently, the baseline $b(\ell/N)$ can be constructed by substituting the above mentioned α and $\beta = 0$ into Equation 9.
2. We generate surrogates of the sequence $\{Y_\ell\}_{\ell=1}^{N}$ and estimate their form error via the following:
    a. Given the estimated A and σ, we adopt the model $\beta_{ij} \sim A \cdot 2^{-\sigma(i-L)} \cdot N(0,1)$ and generate a sequence $u(\ell/N), \ell = 1,2,...,N$ by applying Equation 9 with the above β_{ij}'s and $\alpha = 0$. Let $u^{(k)}(\ell/N), 1 \le \ell \le N$ denote the *k*th generated random sequence.
    b. Define $Y^{(k)}(\ell/N) = b(\ell/N) + u^{(k)}(\ell/N), \ell = 1,2,...,N$, where *b(·)* is generated in step 1, $u^{(k)}(\cdot)$ is generated in step 2a. $Y^{(k)}(\cdot)$ is the *k*th surrogate sequence.
    c. Use the MZ method to estimate the form error of $(\ell/N, Y^{(k)}(\ell/N)), \ell = 1,2,...,N$ and denote it by e_k.
3. Repeat the step 2 for large enough I, and our final form error estimate is the *v*-quantile of the e_k's. Specification on how to decide *v* is given in Appendix B.

Note that both confidence band and form error can be used in quality assessment. We consider them as complimentary methods. Simulations will be performed to study their properties.

3.4 Real Data Study

The assumptions required for our method are verified with the real CMM data in 3.4.1. In 3.4.2, the confidence bands for the data are constructed using the proposed method.

3.4.1 Assumption Verification

We consider data taken both by point-by-point and by scanning. They are plotted in Figure 1. The wavelet transform is carried out. We choose a nearly symmetric wavelet (Symmlet) with six vanishing moments. For each sequence, we extract out a length-512 subsequence. Figure 5 is a standard way to display wavelet coefficients.

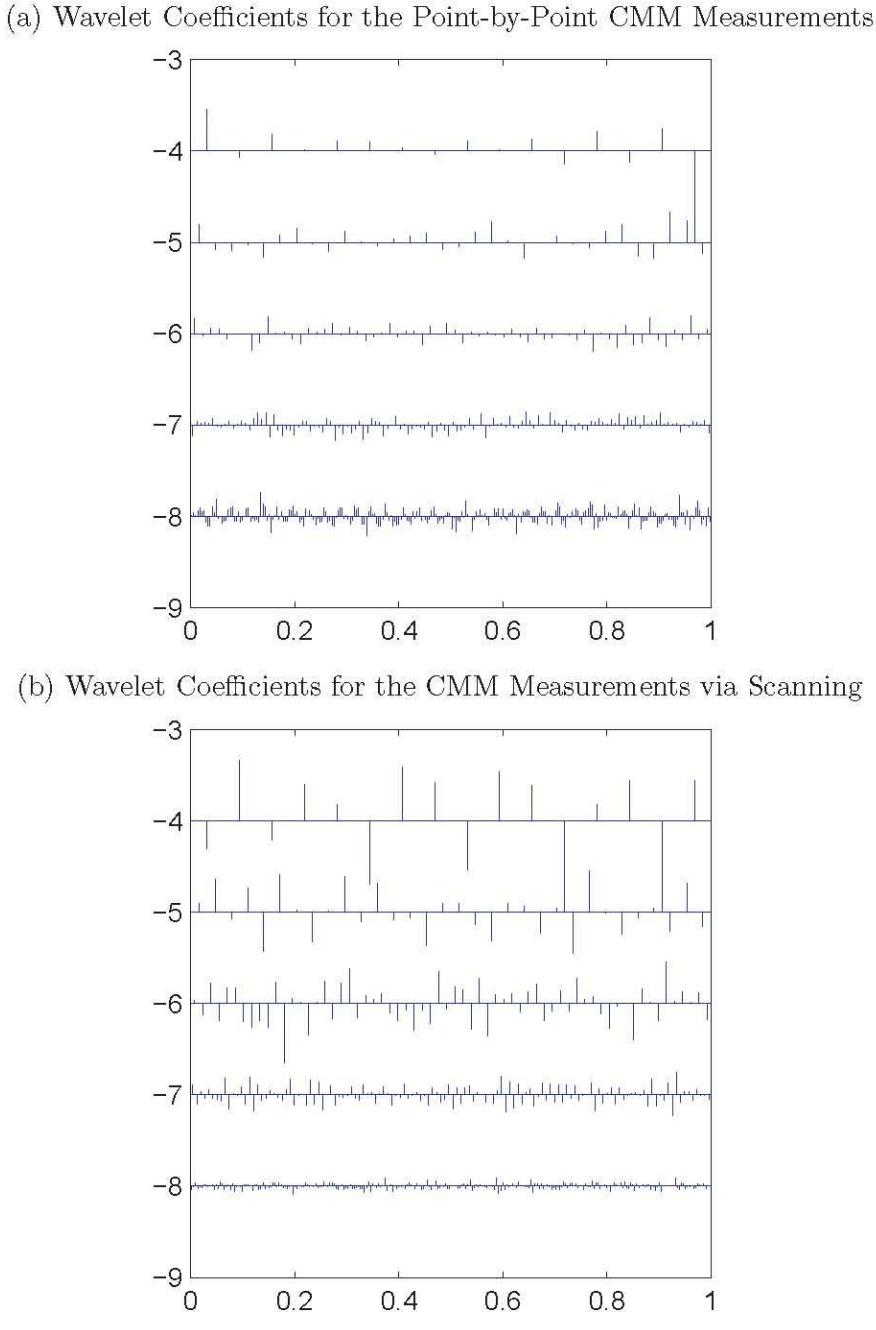

Figure 5: Wavelets Coefficients. Wavelet coefficients at the same scale are plotted on the same horizontal line. All wavelet coefficients are scaled—the stick length is proportional to its absolute value. The horizontal axis represents the location.

Recall Equation 5 is our key assumption. (When Equation 5 holds, by Theorem 2, the underlying function *f(x)* is Lipschitz.) If Equation 5 holds, the maximum absolute value of wavelet coefficients as a function of the scale *i* must be below a decreasing straight line. In Figure 6, we plot the maximum absolute value of wavelet coefficients at all scales. We can clearly see the linear pattern for the scanning data. This experiment has been repeated for different segments of the original signal. The above pattern has been consistently observed. The corresponding figure for the point-by-point case (Figure 6(a)) does not show such a pattern. The likely cause of this difference is the errors associated with repositioning the probe during the point-by-point measurement. We choose the scanning data to examine and measure the smoothness of the surface.

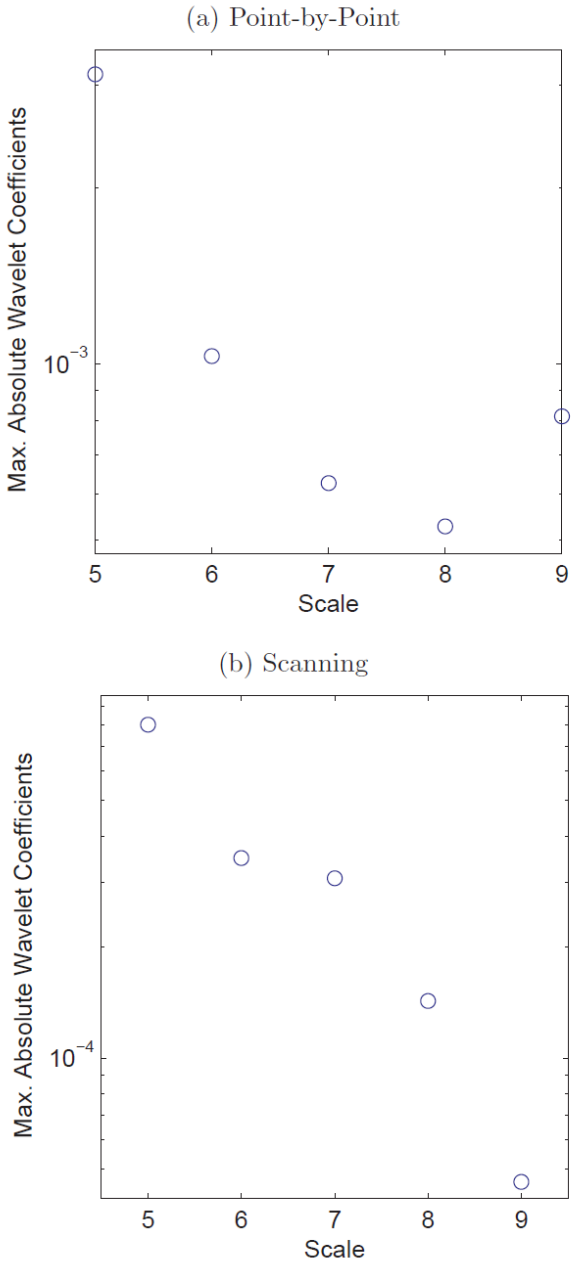

Figure 6: The maximal absolute values of wavelet coefficients per scales versus the scales. The horizontal axis represents the scale. The vertical axis reflects the logarithmic transformed maximum absolute value of wavelet coefficients at each scale. In (b), we observe a decreasing line pattern, which is consistent with Equation 5.

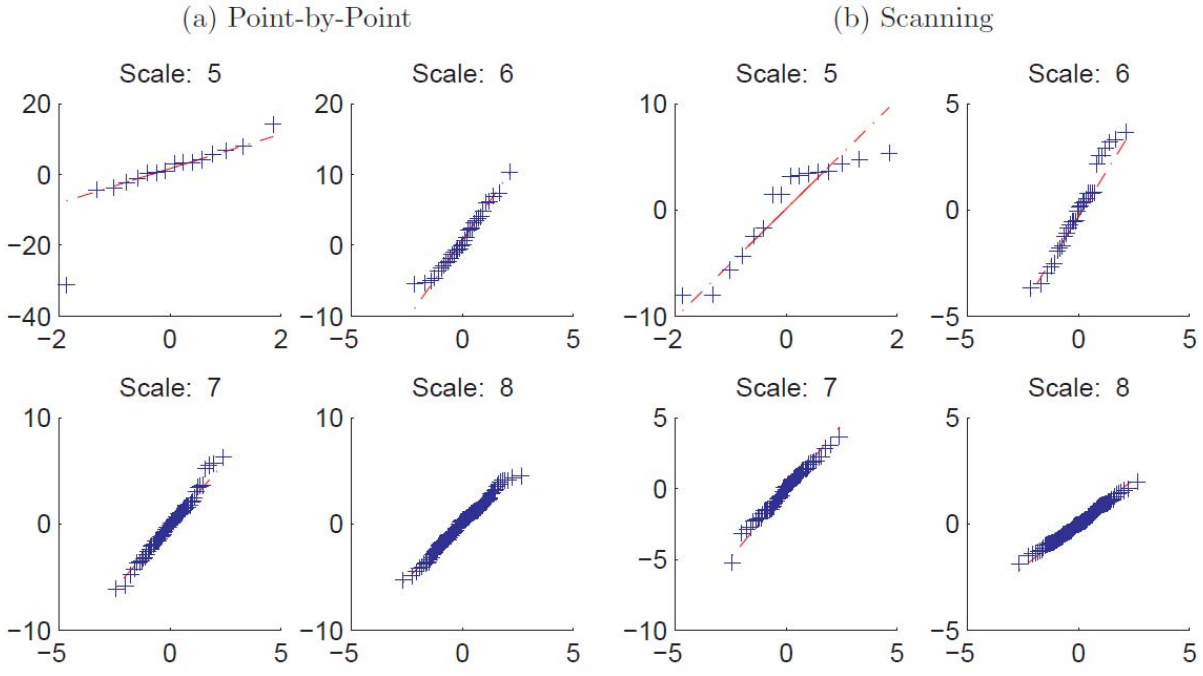

Figure 7: The QQ-plots of the wavelet coefficients at all scales. Each subfigure includes wavelet coefficients at a particular scale.

We study the distribution of the wavelet coefficients at a fixed scale. In Figure 7, the QQ-plots of the wavelet coefficients at the same scale are plotted. The x-coordinates are the standard normal quantiles, while the y-coordinates correspond to the quantiles of the wavelet coefficients at a fixed scale. For illustration purpose, all coefficients are multiplied by 10^4 . Most of the QQ-plots indicate a fit to the normal distributions, except for scale 5 in both cases. For more quantitative results, the Jarque-Bera hypothesis test is run and the corresponding p-values are 0.001, 0.3716, LT5, and LT5 for the four scales in the point-by-point case. (Here LT5 stands for larger than 0.5.) The p-values for the four cases in the scanning measurements are 0.1118, LT5, LT5, and 0.484981. Note the latter case is more interesting, because we study the underlying surface, and the scanning CMM measurements are more faithful to the smoothness of the true surface. The p-values at scale 5 are small (in particular when the point-by-point measurements are considered); however in our framework, the finer scale (i.e., when the scale index is large) is of more interest, because in (2.6), one can increase the value of L by 1, so that the part of the signal associated with scale 5 becomes the part of the signal expressed by the scaling functions (i.e., the first term on the right hand size of (2.6)). In summary, it is reasonable to assume that the wavelet coefficients (β_{ij}) satisfy the normal distribution.

3.4.2 Confidence Bands for CMM Data

We construct the confidence bands for the two CMM data sets that are displayed in Figure 1. Recall that we assume $\beta_{ij} \sim A \cdot 2^{-\sigma(i-L)} \cdot N(0,1)$. We need to estimate A and σ, which correspond to the intercept and slope in Figure 6(b). We apply simple linear regression to obtain the estimates: $\hat{\sigma} = 0.69$ and $\hat{A} = 0.675 \times 10^{-3}$. Applying these parameters, we can determine the half-width of the confidence band via the simulation approach in 3.3.1.2. We found the empirical percentiles (based on 106 simulated sequences) corresponding to 99%, 99.5%, and 99.9% are 5.84×10^{-4} , 6.09×10^{-4}, and 6.62×10^{-4}, respectively. The baseline can be estimated via the aforementioned wavelet shrinkage method. The level 99% and 99.9% confidence bands for each case are displayed in Figure 8.

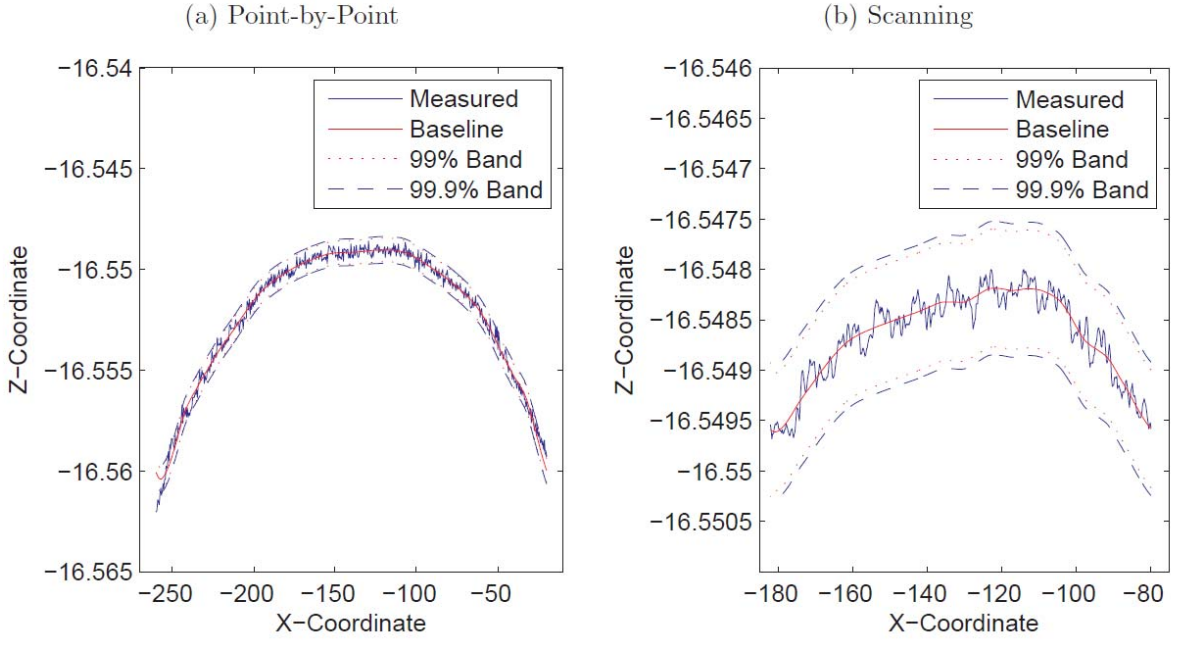

Figure 8: The 99% and 99.9% confidence bands for the CMM measurement displayed in Figure 1. Note that the band is for the underlying surface, not the CMM measurements. The fact that the band barely covers all CMM measurements in (a) may be caused by the large repositioning noise in the point-by-point scheme.

3.5 Simulation Study

We study the confidence band in 3.5.1. The form error estimate is evaluated in 3.5.2.

3.5.1 Simulations on Confidence Bands

In this section, we use synthetic data to examine our method. We will gain insights on our sampling strategy. We assume that the CMM measurement sequence satisfies the model that is proposed in 3.2.4. We set $\sigma = A = 1$. For implementation convenience, we choose the length of sequence N = 512. By doing so, we can take advantage of the existing implementation of the discrete wavelet transforms in WaveLab (http://www-stat.stanford.edu/~wavelab/). We choose the coarsest level to be L = 4. (The choice of L allows subjectivity, which does not hurt the foundation of our model.) As mentioned in model description, we choose Symmlet with six vanishing moments. With these conditions, as discussed in 3.3.2.3, the optimal sampling positions with 16 (= 2^L) points should be 27, 59, 91, 123, 155, 187, 219, 251, 283, 315, 347, 379, 411, 443, 475, and 507. Note that the positions may vary due to differences in the Implementation of the discrete wavelet transform. The above values are based on the implementation in WaveLab.

After taking the measurements at the optimal sampling positions, we estimate the corresponding baseline using the proposed interpolating algorithm in 3.3.2.2. When applying Equation 13, we set $\beta = 0$ (i.e., all fine scale wavelet coefficients are set to be zero) so that the resulting baseline is smooth. We then select the half-width of the confidence band according to the description in 3.3.1.2. Note that with the aforementioned choice of A and σ, the sample percentiles based on one millions simulations are 0.563925(99%), 0.589235(99.5%), and 0.645583(99.9%). There is a caveat in using these quantiles. Note that the resulting confidence band makes sense if the coefficients associated with all scaling functions (i.e. α) are known. Such an assumption is not ralisitic. However, in simulation, one can estimate the pointwise standard deviation of the CMM measurements, using the pointwise standard deviation between the estimated baseline and the simulated sequence. In our case, we found that the estimated pointwise standard deviation ≈ 0.2 so 0.2 is added to the above quantiles. The reason we chose 0.2 instead of e.g., 3×0.2, is that the simulations show the latter is too conservative. More analytical study here is possible to make the width selection more accurate. Figure 9 illustrates one scenario of the above procedure.

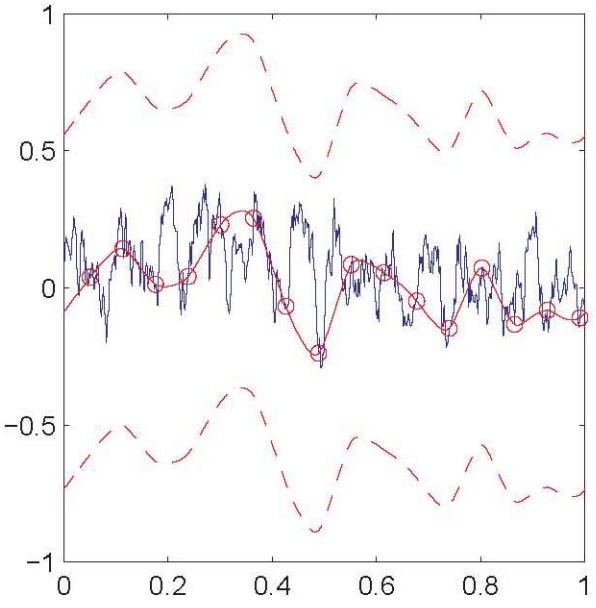

Figure 9: A synthetic example. The noisy curve is simulated data, based on the properties of CMM measurements. Circles indicate positions where measurements are obtained. Two dashed curves circumscribe the 99.9 % confidence band. The fact that the confidence band includes all CMM measurements demonstrates the success of the band.

To validate our proposed confidence band method and our choice of the sampling positions, we carry out numerical studies in the above mentioned framework. Three cases are examined:

(C1) All $2^L = 16$ positions are at the optimal sampling positions that are derived in 3.3.2.3.

(C2) Only part of the previous 16 positions are taken: the 5th, 7th, 9th, and 11th positions are removed. We would like to study the case when the number of samples is less than 2^L, i.e., $n < 2^L$

(C3) Still take 16 sampling positions, however they are not the optimal sampling positions that are specified in 3.3.2.3. We did so by shifting all positions in (C1) to the left by 16. We can also use random sampling positions. Similar results are observed.

Ten thousand experiments are run for each of the above three cases. The number of times that the constructed 99.9 % confidence bands do not cover the generated CMM sequences are 100, 3906, and 5661 for C1 to C3, respectively. We learned the following lessons:

1. Recall one objective is to construct a confidence band (which bases on a small number of measurements), such that this band contains the 'true' surface with high probability. We do

observe that the number of uncovered cases is the minimum in C1. This result validates our construction of the confidence band.

2. The number of uncovered cases in C2 and C3 are significantly larger than the corresponding number in C1. It demonstrates the optimality of our new sampling strategy.

The above leads to the following guideline in adopting our model in practice: making the experimental design conform with C1. For most CMMs, it is not hard to implement this guideline.

3.5.2 Comparison with Traditional Methods

In this subsection, we estimate form error as described in 3.3.3, and compare the results with the two traditional methods: the Minimum Zone (MZ) method and the Orthogonal Least Squares (OLS) method. For the comparison, we focus on the unbiasedness of the form error estimates (similar to Xia et al. (2008)). We calculate the ratios of the estimated form errors over the true form errors; note that the estimate is less biased if the calculated ratio is closer to one. The specific procedure is as follows.

Step 1. Simulate a dense enough set of measurements. Specifically, set N = 512, σ = A = 1, L = 4, and generate the function as $y = \Phi_1\alpha + \Phi_2\beta$, where $\beta_{ij} \sim A \cdot 2^{-\sigma(i-L)} \cdot N(0,1)$ and $\alpha_j = 0, \forall j$.

Step 2. Specify a potential tolerance τ for part acceptance. For this, generate 1000 functions as in Step 1. Let m_i denote the maximum magnitude in the ith function. We choose τ as $\tau = 1.5 \times \max_i m_i$.

Step 3. Add measurement errors to y in Step 1. That is, $y = \Phi_1\alpha + \Phi_2\beta + \varepsilon \cdot N(0,1)$, where ε incorporates the errors of individual CMM measurement. We choose $\varepsilon = \tau/5$. (It is a reasonable requirement that the measurement equipment uncertainty must be 5 times smaller than the tolerance zone). Determine the form error using the MZ method, and treat it as the "true" form error.

Step 4. From the measurements in Step 3, take the small number of samples using the sampling approach C1 ~ C3.

Step 5. Using the samples taken in Step 4, estimate form error using the three different methods (MZ, OLS, and our method), and calculate the ratios of the estimated form errors over the true form error.

Table 1 compares the calculated ratios from the three methods. The values in parentheses are standard errors. Both MZ and OLS underestimate the form error. Our method is less biased. Xia et al. (2008) compares Gaussian process (GP) models with MZ and OLS as well. By comparing to their results, we believe that GP and our method will render similar performance.
Table 1 reconfirms that C1 is the best sampling strategy under our model.

	MZ	OLS	Our method
C1	0.5618 (0.1279)	0.5912 (0.1370)	0.9904 (0.1287)
C2	0.5084 (0.1353)	0.5350 (0.1432)	0.9378 (0.1252)
C3	0.5889 (0.1245)	0.6184 (0.1315)	1.7426 (0.4507)

Table 1: MZ, OLS, and our method are compared for the unbiasedness of the form error estimation. The averaged ratios based on 1000 simulations are shown. The standard errors are in the parentheses.

3.6 Discussion

We aim at developing a general theory on the construction of the confidence band, form error assessment, and the sampling strategy based on this model. In testing the measurement compliance with the requirements and determining sampling positions, none of the existing works considers the wavelet-based model. We are the first to utilize Lipschitz property to establish a statistical model for CMM measurements. Our data-driven approach to identify a statistical model represents a trend in modern functional data analysis. The proposed work differs from existing basis function approaches (which may uses wavelets as basis functions): we use the wavelet framework as an intermediate tool to create a statistical model for Lipschitz functions, while most existing work uses wavelets as a nonparametric smoothing tool. In the proposed model, specific types of wavelets (i.e., not all types of wavelets) must be adopted; our treatment of wavelet coefficients is different from other methods when wavelets are merely used for smoothing.

Extension to 2-D. So far, we have discussed the case when the underlying boundary is a 1-D function f residing in the unit interval [0,1]. It can be straightforwardly extended to 2-D surface,

if we can assume that the 2-D surface is a tensor production of two 1-D functions; although in reality, such an assumption may be too optimistic. Tensor production simply implies that $h(x,y) = f(x) \cdot g(y), x, y \in [0,1]$, where *f(x)* and *g(y)* are uniformly Lipschitz $\gamma > 0$. The assumption of tensor production really simplifies the derivation. Most of the algorithm in 2-D is nearly parallel with the algorithm in 1-D. However, 2-D is a much more delicate problem than 1-D. See related works: [8, 25, 26]. To consider 2-D problems, one may subtract an estimated form from the measurements, so that the problem is converted into a straightness problem.

3.7 Conclusion

This section describes a wavelet-based method to construct confidence bands, to assess form errors, and to determine a sampling strategy for CMM measurements in coordinate metrology. The confidence band for the measurement data is computed via specifying its baseline and the half-width of the confidence band; the former can be constructed via the wavelet shrinkage method, and the latter can be obtained via simulation based on the Lipschitz regularity. For the form error assessment, we predict the surface of the geometric feature (a dense set of measurements) using a small number of observed samples, and find the maximum inscribing and minimum circumscribing geometry that bounds all points on the predicted surface. For the sampling strategy, a wavelet-based random curve interpolating algorithm is considered. We discuss the optimal choice of new sampling positions under our model. The proposed method has been validated with synthetic and real data.

Although this method shows good results, especial with regard to establishing a confidence bound, there are a few problems with implementation in a production setting. First, the sampling points chosen are optimal for the wavelet-based model only, which turns out to be a uniform sampling strategy. Uniform sampling strategies have been found to be non-optimal [7], [6] when used to measure manufactured parts. Second, the mathematics used to calculate confidence intervals is fairly complicated, which may lead to difficulty in adopting this method in production. Because of these problems, the implementation of adaptive sampling on a commercial CMM was also explored.

4 Adaptive Sampling Method

4.1 Background

The adaptive sampling discussed is limited to CMMs, although the general ideas should be applicable with other measurement disciplines.

Reducing the number of points being measured is desirable, because it speeds throughput. An adaptive program determines if a higher point density is required in a local region, then, increases the density in that region. The higher point density in a local region captures variability in the measured surface. If the surface does not exhibit 'sufficiently large' variability, then, there is no need to increase the point density. The limitation with adaptive sampling is that it will not capture pathological errors, such as nicks.

Measurements on a CMM take time. Therefore, by reducing the sampling density the increased sampling is not necessary, measurement time is reduced, compared to a uniform high density sampling. The cost function with operation of a CMM is primarily machine time. We can state this desire as an effort to minimize the number of points taken.

Adaptive algorithms have a long research history. Edgeworth and Wilhelm [8] proposed an adaptive sampling strategy which uses an iterative process to select and analyze measurement points. The measurement data are used to develop an interpolating curve which is then used to select subsequent measurement points. The process continues until the measurement converges, with more accurate parts requiring fewer measurement points and less accurate parts requiring more. Application of adaptive sampling is limited, in part because programming methods for typical CMMs can make this type of iterative measurement difficult to implement. We consider the feasibility of programming a CMM to implement an adaptive sampling strategy in Section 4.

Rossi [27] describes an adaptive sampling method for measuring roundness using a CMM. A strategic distribution of initial sampling points allows for detection of waviness and random deviation, two frequent categories of profile error. Based on the type of error determined from the initial points, additional points are measured in order accurately measure the roundness with

a minimum of points. This method is presently limited to roundness evaluation and the accuracy is dependent on correctly identifying the type of deviation present.

Pedone et al. [28] apply a kriging model, developed to predict spatial data in geostatistics, to CMM inspections. The kriging model is used to predict the surface pattern at each step in the sampling routine. This model is tested on measurements of straightness and roundness. The results show two advantages to using this method; first, like other adaptive sampling plans, the quality of the part drives the number and location of sampling points, second, the prediction allows for a statistical, model-based, evaluation of form error.

Badar et al. [29] apply several optimization search methods in order to reduce the sample size. An initial set of points is pre-determined. The next points sampled are based on measured points and the search method used, with the goal of improving the accuracy of the fit zone. The results show good accuracy with a smaller size than has been typically recommended in the literature. This paper used CMM data in simulation, rather than programming the CMM.

4.2 Methodology

We have decided to implement a well known adaptive algorithm based on adaptive quadrature (evaluation of a definite integral) in order to evaluate the feasibility of implementing an adaptive sampling routine on a CMM. The estimated error in evaluating a definite integral becomes smaller as the density of evaluated points is increased; however, the cost of computing the integral also increases as the point density increases. Adaptive quadrature attempts to increase the density of points where the function to be integrated exhibits exhibits large changes in curvature, and does not increase the density of points where the function is relatively straight. This very much parallels the desire for adaptive sampling along a line segment for a CMM (or, with suitable coordinate transformation, a segment along an arc). We therefore chose to parallel the development of QUANC8 [30], a robust and well-known adaptive quadrature algorithm.

QUANC8 uses, as its basis, an 8 point quadrature formula. If the error estimate for the integral is not reached, an additional 8 points are added. A notable feature of QUANC8 is that the points where the function is evaluated are reused; that is, when the point density is increased, only the additional points are evaluated. This minimizes the number of function evaluations (which is a major cost driver in numerical analysis).

For adaptive sampling on a CMM, we decided to evaluate a line segment, as the logic is relatively easy to develop, and readily implementable on commercial CMM software.

The user needs to make assumptions that the segment being measured is not pathological (nicks or divots). Given some desired criteria for geometry of a line (maximum deviation of line, or form, does not exceed a particular value), the algorithm is as follows:

A. Sample a line (use 17 pts) (note that density = L/(n-1))
B. Do you meet global convergence (max-min)? If yes, stop, else
C. Divide into half-segments, 1-9 and 9-17 (note we reuse pt 9 in between)
D. Check left half-segment.
E. Does it meet local convergence (max-min)/scale? If yes, go to right half, else
F. Have you met maximum point density? If yes, stop, else
G. Add 8 pts to segment and measure (no evaluation) these pts. Collect together the 8 newly measured pts & the 9 older pts.
H. Divide into half-segments, 1-9 and 9-17.
I. Check left half-segment.
J. Does it meet local convergence (max-min)/scale? stop, else
K. If max density reached, stop, else
L. Divide into half-segments, 1-9 and 9-17
M. Resample & re-evaluate half-segment (per (1) and (2))
N. Repeat for right-half segments.

This is illustrated in the sketch of Figure 10. The choice of 17 initial points with half-segments of 9 points (8 intervals) each was arbitrary. Any choice of a power of 2 for the numbers of intervals in each half-segment would work. Note that when the density is increased, it is only necessary to measure the added points. With CMMs, computing and evaluating are much faster than performing the actual measurement. Therefore, reusing points is a useful feature.

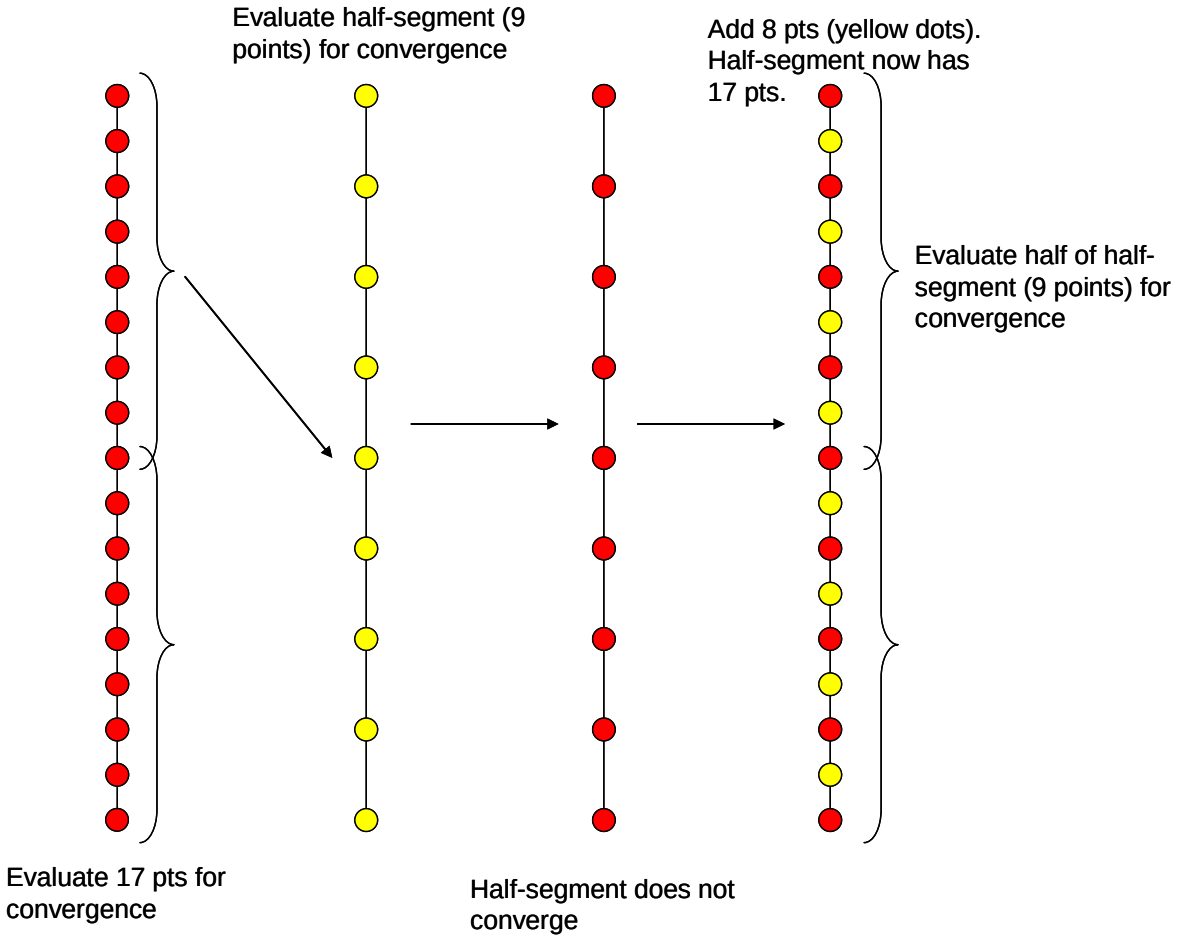

Figure 10: Adaptive sampling method.

4.3 Simulation

Before implementing the proposed adaptive sampling method on a CMM, it was simulated in MATLAB in order to check the routine and make observations. Two hundred sixty seven points were taken along a straight edge on the CMM (see Section 4.4). The simulation evaluates subsets of these measured points according to the method described above.

The simulation first chose 17 evenly spaced points (red in Figure 11) from the measured set of 257 points (black in Figure 11). A line was fit through the 17 points (solid blue). The maximum distance from the line to one of the 17 points was calculated and compared to the convergence criteria (dashed blue lines, zone = 3 μm wide). Because at least one point does not meet the convergence criteria, the line is divided into two halves and the routine continues.

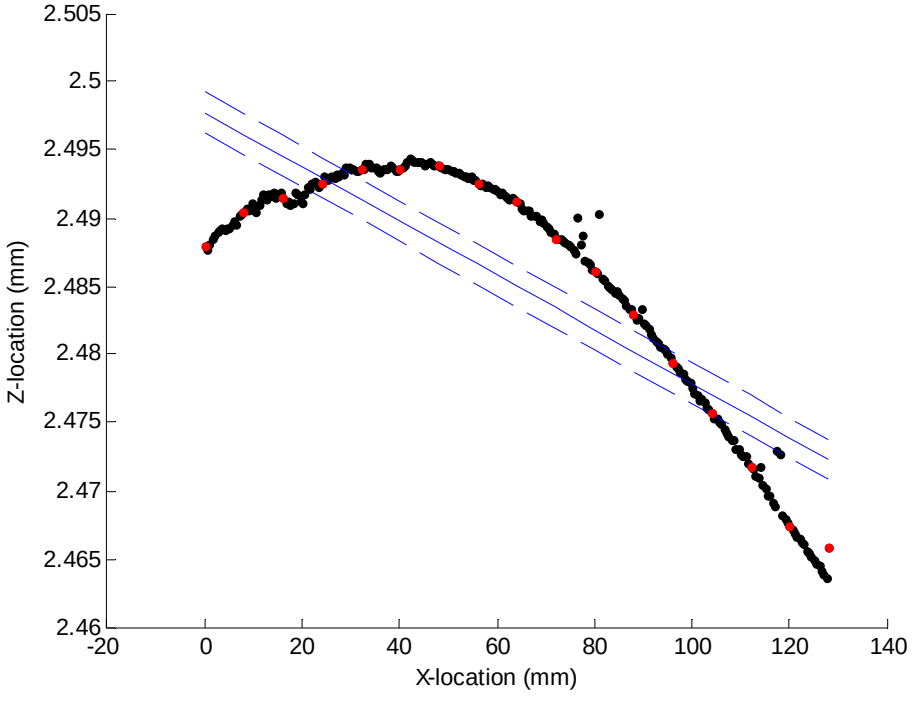

Figure 11: Initial fit using 17 points.

Each of the two halves (9 points) are evaluated separately, see Figure 12. The right half meets the convergence criteria so it is not further subdivided. The left half does not meet the convergence criteria so it is subdivided.

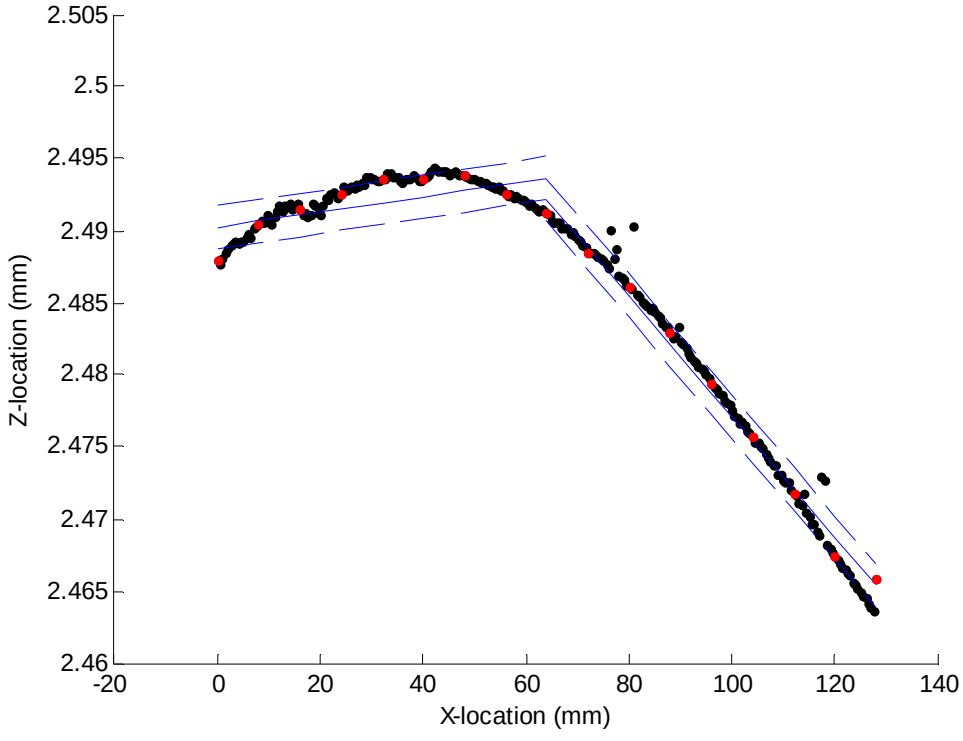

Figure 12: Evaluate left and right halves separately, note that right side is within prescribed zone, left side is not.

Points are added between the already existing 9 points on the left half to make a total of 17 points. The 17 points are divided into left and right halves and evaluated to determine if they meet the convergence criteria (Figure 13). Both the left and the right halves meet the convergence criteria, so there are no further subdivisions.

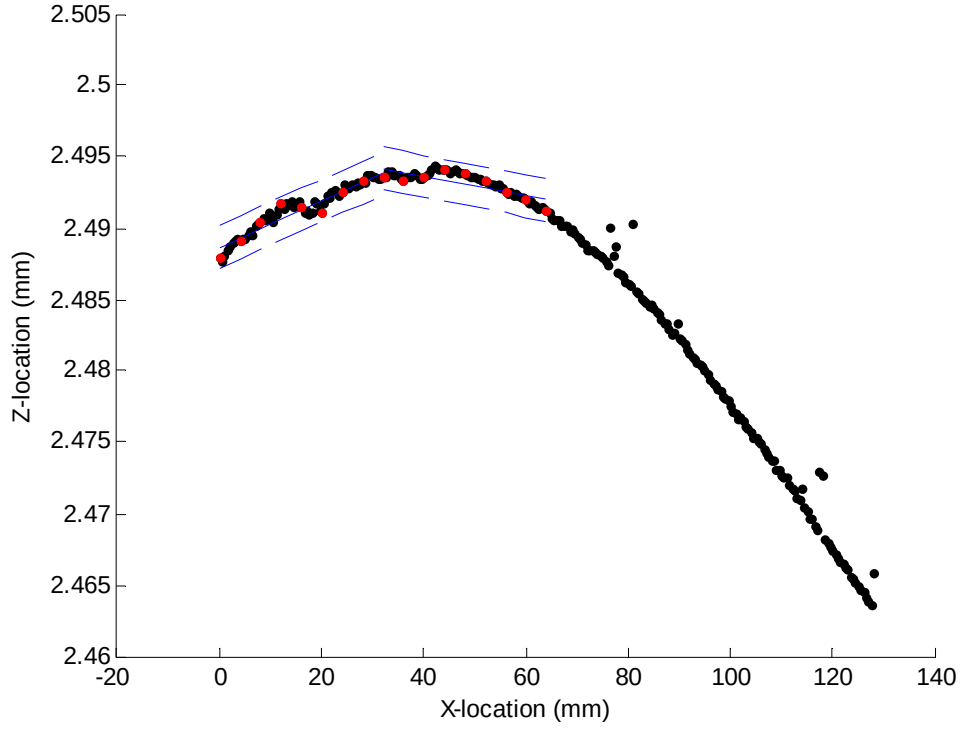

Figure 13: Subdivision of left side, all points now within prescribed zone.

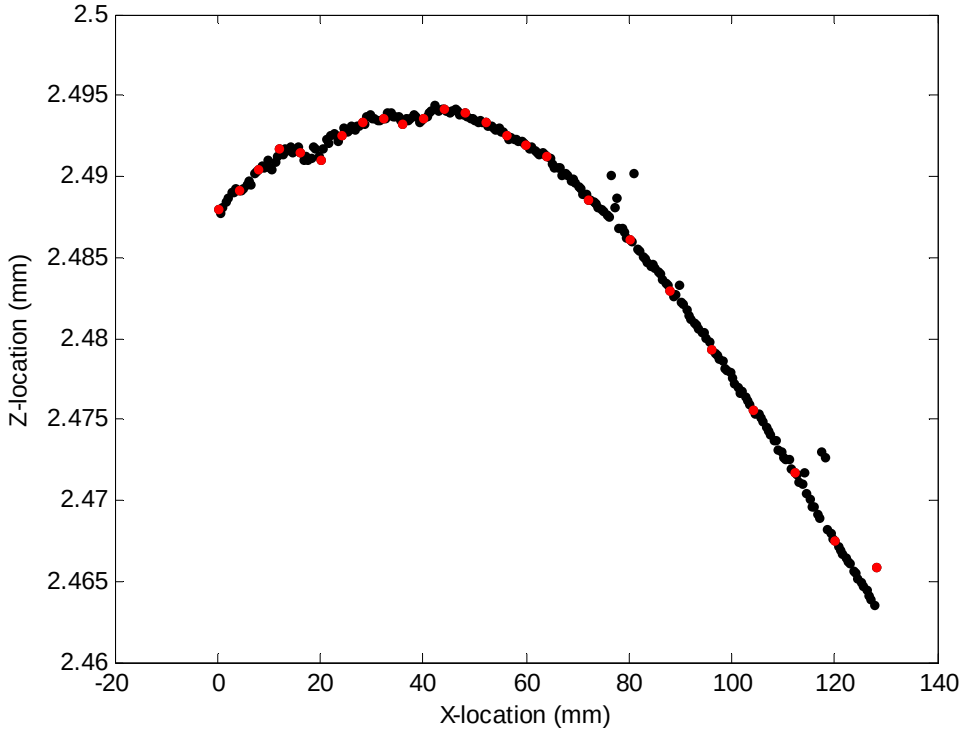

Figure 14: Points selected during simulation (red) compared to all measured points (black).

If the convergence criterion is changed, for example to a zone of 2 μm from the 3 μm previously used, the sampled points change. Figure 15 illustrates this change. With a convergence zone of 3 μm, 25 points are sampled. With a convergence zone of 2 μm, 73 points are sampled. On the right hand side of the curve, the convergence zone criterion was never met; instead the maximum point density criterion was met.

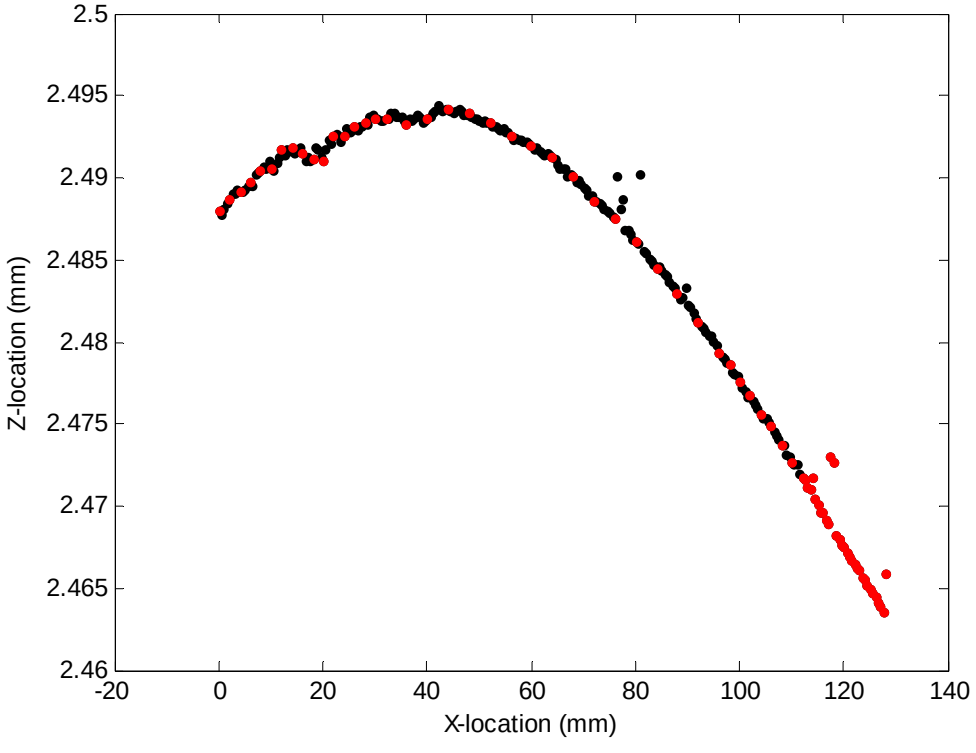

Figure 15: Sampled points using convergence zone of 2 μm.

4.4 CMM Implementation

The above algorithm was developed with CMM implementation in mind, but actual code to perform adaptive sampling was not written on the CMM. Data was collected on a Hexagon Metrology Leitz PMM-C-Infinity 12.10.6 in Sandia National Laboratories' Primary Physical Standards Length/Mass/Force laboratory. This Leitz CMM uses Quindos v6 and Quindos v7 as programming languages. Any CMM programming language with the following features could be programmed to perform adaptive sampling[‡]:

- Conditional branching and looping

[‡] Zeiss Metrology's *Calypso*, OGP's *MeasureMind*, and Hexagon's *PC-DMIS* all have these features.

- Real variables separate from geometry elements
- Storage of data of measured points, independently of evaluation
- Separating and combining sets of points for evaluation

In order to generate the data points used in the simulation, a steel parallel (1”×2”×12”) was used as a straightedge. The parallel was mounted on the CMM table, but a shim was placed under the parallel to induce curvature in the parallel. A line segment 128 mm long was measured at 0.5mm intervals (256 intervals, 257 points). The points were exported to ASCII text for evaluation and simulation in MATLAB (as in Section 4.3).

Some example Quindos commands which would be used for adaptive sampling are tabulated below.

Algorithm step	**Quindos commands to be used**

Sample a line (use 17 pts) (note that density = L/(n-1)). In this case, the entire segment is AX, going from the value XMIN to XMAX, with 16 intervals (17 points).	GENAXI to generate the points:
	`GENAXI (NAM=AX, XBG=XMIN, YBG=0, ZBG=0, XCE=XMAX, YCE=0, ZCE=0, NPT=17, DIR=CSY$B.$ZDI, DEL=Y)`
	
	MEAXI to measure the points
	`MEAXI (NAM=AX, ITY=GSS, PTY=ZX, CTY=ZM)`

Do you meet global convergence (max-min)? If yes, stop, else	IF statements. IF executes subroutines depending on result, IFGOTO jumps to a program line depending on result, IFTHEN/ELSEIF/ENDIF provides an IF/THEN/ELSE structure.

Divide into half-segments, 1-9 and 9-17 (note we reuse pt 9 in between). The two half-segments are AXA and AXB. They are created from the existing geometric element AX. The 'MOD=NOM' option is a flag to specify not to repeat the physical measurements (the points of AX have already been measured).	`COLAPT (NAM=AXA, DEL=N, PTS=AX, FRS=1, LST=9, TYP=AXI)`
	
	`MEAXI (NAM=AXA, MOD=NOM, CDI=-CSY$B.$ZDI, ITY=GSS, PTY=ZX, CTY=EX)`
	
	`COLAPT (NAM=AXB, DEL=N, PTS=AX, FRS=9, LST=17, TYP=AXI)`
	
	`MEAXI (NAM=AXB, MOD=NOM, CDI=-CSY$B.$ZDI, ITY=GSS, PTY=ZX, CTY=EX)`
	
	The COLAPT command can be used to create new geometric elements from a single existing geometric element, or from a combination of existing geometric elements.

Check half-segment (AXA in this example). The form value LFTFORM is the maximum deviation from the best fit least square line minus the minimum deviation from the fit line.	Form value is `LFTFORM=AXA.ACT.ABS.DI.Y-AXA.ACT.ABS.DI.X` Note that the line segment AXA is a geometric element, and is stored in Quindos as a data structure. LFTFORM is a real variable which is calculated by taking the maximum deviation minus the minimum deviation.

Algorithm step	Quindos commands to be used
Add 8 pts to segment and measure (no evaluation) these pts. Collect together the 8 newly measured pts & the 9 older pts.	GENAXI to generate the new 8 points MEAXI, option MOD=NOE (no evaluation) COLAPT to combine points (8 new, 9 existing) into the new, higher density 17 point segment MEAXI, option NOM (evaluate, but don't re-measure)

4.5 Conclusions

We have demonstrated the feasibility of programming an adaptive sampling subroutine on existing CMM software. This demonstration is limited to one-dimensional geometry, such as lines, or, with suitable change of coordinates, arcs or curves. Using experimentally obtained data, the proposed adaptive sampling algorithm correctly increases sampling density where the measured line segment has greater curvature than where the measured line segment is straighter. The logic in the adaptive sampling algorithm is readily implementable on commercial CMM software. We believe that implementing the algorithm described above would be a useful addition to existing CMM line segment measurement methods, which are all based on uniform density sampling. The MATLAB algorithm for adaptive sampling that has been developed can be used for quantitative offline evaluation of scanned point data. The offline evaluation could suggest where higher densities are needed when formulating measurement inspection plans during pilot manufacturing phase.

Extension to two-dimensions for surfaces is a more complicated problem. Consider the simple extension of the adaptive quadrature method to two dimensional surfaces, using Cartesian grid areas that can be subdivided: While a two-dimensional adaptive algorithm based on this appears straightforward, it oversamples two-dimensional surfaces. Triangular grids provide the least number of points that can uniformly sample a surface, but programming triangular areas and subdividing them is more challenging. We believe that two-dimensional adaptive sampling methods may be drawn from the extensive research literature in adaptive meshing for finite element analysis methods.

5 References

[1] Y. Ding, et al., "Distributed sensing for quality and productivity improvements", *IEEE Transactions on Automation Science and Engineering*, 3, pp. 344-359, 2006.

[2] C. Liu, Y. Ding, and Y. Chen, "Optimal coordinate sensor placements for estimating mean and variance components of variation sources", *IIE Transactions*, 37, pp. 877-889, 2005.

[3] "Coordinate measuring machines and systems, ed. J.A. Bosch. New York: Marcel Dekker, 1995.

[4] B.M. Colosimo, G. Moroni, and S. Petro, "A tolerance interval based criteron for optimizing discrete point sampling strategies", *Precision Engineering*, 34, pp. 745-754, 2010.

[5] K.-C. Fan and M.C. Leu, "Intelligent planning of CAD-directed inspection for coordinate measuring machines", *Computer Integrated Manufacturing Systems*, 11, pp. 43-51, 1998.

[6] C. Prakasvudhisarn and S. Raman, "Framework for Cone Feature Measurement Using Coordinate Measuring Machines", *Journal of Manufacturing Science and Engineering*, 126, pp. 169-177, 2004.

[7] G. Lee, J. Mou, and Y. Shen, "Sampling strategy design for dimensional measurement of geometric features using coordinate measuring machine", *International Journal of Machine Tools and Manufacture*, 37, pp. 917-934, 1997.

[8] R. Edgeworth and R.G. Wilhelm, "Adaptive sampling for coordinate metrology", *Precision Engineering*, 23, pp. 144-154, 1999.

[9] K.D. Summerhays, et al., "Optimizing discrete point sample patters and measurement data analysis on internal cylindrical surfaces with systematic form deviations", *Precision Engineering*, 26, pp. 105-121, 2002.

[10] G. Zhang, et al., "Error Compensation of Coordinate Measuring Machines", *CIRP Annals*, 34, pp. 445-448, 1985.

[11] M.M. Dowling, et al., "Statistical issues in geometric tolerance verification using coordinate measuring machines", *Technometrics*, 39, pp. 1-24, 1997.

[12] L.P. Rivest, "Some linear models for estimating the motion of rigid bodies with applications to geometric quality assurance", *Journal of the American Statistical Association*, 93, pp. 632-642, 1998.

[13] H. Xia, Y. Ding, and J. Wang, "Gaussian process method for form error assessment using coordinate measurements", *IIE Transactions*, 40, pp. 931-946, 2008.

[14] S. Mallat, "A wavelet tour of signal processing. San Diego, CA: Academic Press, 1998.

[15] A. Slocum, "Precision Machine Design. Upper Saddle River, NJ: Prentice-Hall, 1992.

[16] ASME B46.1,*Surface Texture, Surface Roughness, Waviness, and Lay*, 2001.

[17] D. Whitehouse, "Surfaces and Their Measurement,. London, UK: Hermes Penton Science, 2002.

[18] J. Tlusty, "Manufacturing Processes and Equipment. Upper Saddle River, NJ: Prentice-Hall, 2000.

[19] H.Q. Zheng, et al., "Theoretical Modelling and Simulation of Cutting Forces in Face Milling with Cutter Runou", *International Journal of Machine Tools and Manufacture*, 39, pp. 2003-2018, 1999.

[20] T.L. Schmitz, et al., "Case study: A comparison of error sources in high-speed milling", *Precision Engineering*, 32, pp. 126-133, 2008.

[21] M.P. Groover, "Fundamentals of Modern Manufacturing: Materials, Processes, and Systems. Hoboken, NJ: John Wiley & Sons., 1999.

[22] D.L. Donoho and I.M. Johnstone, "Adapting to unknown smoothness via wavelet shrink¬age", *Journal of the American Statistical Association*, 90, pp. 1200-1224, 1995.

[23] ASME B89.7.3.1,*For Decision Rules: Considering Measurement Uncertainty In Determining Conformance To Specifications*, 2001.

[24] ANSI Z540.3,*Requirements for the Calibration of Measuring and Test Equipment*, 2006.

[25] C.E. Collins, et al. "Alternate methods for sampling in coordinate metrology" in *Proceedings of the Institution of Mechanical Engineers Part B-Journal of Engineering Manufacture*, 2007.

[26] R.C. Gilbert, et al., "Mathematical foundations for form inspection and adaptive sampling", *Journal of Manufacturing Science and Engineering-Transactions of the ASME*, 131, pp. 041001, 2009.

[27] A. Rossi, "A form of deviation-based method for coordinate measuring machine sampling optimization in an assessment of roudness", *Proceedings of the Institution of Mechanical Engineers; Part B; Journal of Engineering Manufacture*, 215, 11, pp. 1505-1518, 2001.

[28] P. Pedone, G. Vicario, and D. Romano, "Kriging-based sequential inspection plans for coordinate measuring machines", *Applied Stochatic Models in Business and Industry*, 25, 2, pp. 133-149, 2009.

[29] M.A. Badar, S. Raman, and P. Pulat, "Intelligent search-based selection of sample points for straightness and flatness estimation", *Journal of Manufacturing Science and Engineering*, 125, pp. 263-271, 2003.
[30] G.E. Forsythe, M.A. Malcom, and C.B. Moler, "Computer Methods for Mathematical Computations. Englewood Cliffs, NJ: Prentice-Hall, Inc., 1977.

Appendix:

A Proof of Lemma 1

Proof. Writing the condition in (3.12) in a generic form, we have

$$\min \|\alpha\|_2^2, \quad \text{subject to } A\alpha = b$$

where A is a matrix of full row rank and **b** is a vector. We consider its Lagrangian:

$$L(\alpha, \lambda) = \alpha^T \alpha + \sum_{i=1}^{r} \lambda_i (A_i \alpha - b_i) = \alpha^T \alpha + \lambda^T (A\alpha - b)$$

where λ_i is the ith Lagrangian multiplier, which is also the ith component of vector λ, A_i is the ith row of A, and b_i is the ith entry of b. The above achieves minimum if and only if

$$\begin{cases} 2\alpha + A^T \lambda = 0 \\ A\alpha = b \end{cases}$$

The above can be rewritten as

$$\begin{pmatrix} 2I & A^T \\ A & 0 \end{pmatrix} \begin{pmatrix} \alpha \\ \lambda \end{pmatrix} = \begin{pmatrix} 0 \\ b \end{pmatrix}$$

Hence we have

$$\begin{pmatrix} \alpha \\ \lambda \end{pmatrix} = \begin{pmatrix} 2I & A^T \\ A & 0 \end{pmatrix}^{-1} \begin{pmatrix} 0 \\ b \end{pmatrix}$$

Notice that we have

$$\begin{pmatrix} 2I & A^T \\ A & 0 \end{pmatrix}^{-1} = \begin{pmatrix} \frac{1}{2} I - \frac{1}{2} A^T \left(AA^T\right)^{-1} A & A^T \left(AA^T\right)^{-1} \\ \left(AA^T\right)^{-1} A & -2\left(AA^T\right)^{-1} \end{pmatrix}$$

which brings us the following closed-form solution

$$\begin{pmatrix} \alpha \\ \lambda \end{pmatrix} = \begin{pmatrix} A^T \left(AA^T\right)^{-1} b \\ -2\left(AA^T\right)^{-1} b \end{pmatrix}$$

For our purpose, we have $A = \Phi_1$ and $b = y - \Phi_2 \beta$, which leads to Equation 13.

Determination of ν in Section 3.3.3

We consider how to determine *v*, such that the resulting estimator is unbiased. Based on our statistical model, ν depends on three sets of parameters: (1) A and σ reflecting the smoothness of the surface, (2) ε, standard deviation of the measurement errors (same notation as in step 3 in 3.5.2), and (3) α, coefficients of the scaling functions, reflecting the shape. It is hard to derive the value of *v* analytically. We use simulations instead. *A* and σ are estimable via scanning data; corresponding strategy has been discussed in 3.4.1. For ε, one can first take the differences of neighboring CMM measurements, then consider the median absolute value (MAD) statistic as an estimator. If straightness is the target, we can simply take $\alpha = 0$.

When A, σ, ε, and α are given, simulations can be used to choose *v*. Let N_1 denote the total number of random *y*'s that are generated (similar to the Step 1 in 3.5.2). Let N_2 denote the number of surrogates (whose generation is described in Step 2 in 3.3.3). Furthermore, let e_{ij} denote the form error of the *j*th surrogate in the *i*th experiment, $i = 1,...,N_1, j = 1,...,N_2$. Let e_{i0} denote the computed form error for the *y* in the *i*th experiment. Without loss of generality, we assume that for fixed *i*, e_{ij}'s are nondecreasing as *j* increases. We find the *j* that solves

$$\min_{j:1\le j\le N_2} \sum_{i=1}^{N_1} \left| \frac{e_{ij}}{e_{i0}} - 1 \right|$$

The above is to find the empirical quantile, such that the corresponding e_{ij}'s are closest to the e_{i0}'s. The j^*/N_2 (with j^* being the minimizer) is the desirable value of *v*. In our experiments in 3.5.2, by using the estimated parameters $\hat{A} = 1.0444, \hat{\sigma} = 0.9720, \hat{\varepsilon} = 0.2013$, and setting $\alpha = 0$, we found that ν =0.974, which is used in our simulations.

Distribution

1 Georgia Institute of Technology (electronic copy)
Attn: Xiaoming Huo (xiaoming@isye.gatech.edu)
School of Industrial and Systems Engineering
765 Ferst Drive, NW
Atlanta, GA 30332-0205

1 MS0613 S. G. Barnhart, 02540 (electronic copy)
1 MS0665 E. H. Detlefs, 02541 (electronic copy)
1 MS0665 K. M. Shilling, 02541 (electronic copy)
1 MS0665 H. D. Tran, 02541 (electronic copy)
1 MS1451 A. J. Medina, 02500 (electronic copy)
1 MS0899 Technical Library, 09536 (electronic copy)
1 MS0359 D. Chavez, LDRD Office, 01911 (electronic copy)


Sandia National Laboratories